Quantitative analysis of stylolite networks in different platform carbonate facies

Elliot Humphrey[1], Enrique Gomez-Rivas[2,1], Joyce Neilson[1], Juan Diego Martín-Martín[2], David Healy[1], Shuqing Yao[1] and Paul D. Bons[3,4]

(1) School of Geosciences, King's College, University of Aberdeen, AB24 3UE Aberdeen, United Kingdom
(2) Departament de Mineralogia, Petrologia i Geologia Aplicada, Facultat de Ciències de la Terra, Universitat de Barcelona (UB), Martí i Franquès s/n, 08028 Barcelona, Spain
(3) China University of Geosciences (Beijing), Xueyuan Road 29, Haidian district, 100083 Beijing, China
(4) Department of Geosciences, Tübingen University, Wilhelmstr. 56, 72074 Tübingen, Germany

Corresponding author: Humphrey, E.: Department of Geology and Petroleum Geology, School of Geosciences, University of Aberdeen, Meston Building, King's College, Aberdeen AB24 3UE, Scotland, United Kingdom; + 44 (0) 1224 273915; e.humphrey@abdn.ac.uk

Keywords: Stylolite, Carbonate, Diagenesis, Lithofacies, Mechanical stratigraphy, Maestrat Basin.

Abstract
Stylolites are rough surfaces that form by pressure solution, and present variable geometries and spatial distributions. Despite being ubiquitous in carbonate rocks and potentially influencing fluid flow, it is not yet clear how the type and distribution of stylolite networks relate to lithofacies. This study investigates Lower Cretaceous platform carbonates in the Benicàssim area (Maestrat Basin, Spain) to statistically characterize stylolite morphology and stylolite network distributions in a selection of typical shallow-marine carbonate lithofacies, from mudstones to grainstones. Bedding-parallel stylolite networks were sampled in the field to quantify stylolite spacing, wavelength, amplitude, intersection morphology and connectivity. Grain size, sorting and composition were found to be the key lithological variables responsible for the development of rough anastomosing stylolite networks. Poorly-connected stylolites with large vertical spacings were found to be dominant in grain-supported lithofacies, where grains are fine and well sorted. Anastomosing stylolite networks appear well developed in mud-supported lithofacies with poorly-sorted clasts that are both heterogenous in size and composition. Mud-supported facies feature stylolites that are closely spaced, have high amplitudes and intersection densities, and predominantly present suture and sharp-peak type morphologies. Larger grains and poor sorting favour the formation of stylolites with small vertical spacings, low wavelengths and high amplitudes. This statistical analysis approach requires only limited information, such as that from drill core, and can be used to characterise stylolite morphology and distributions in subsurface carbonate reservoirs.

This manuscript is published in Marine and Petroleum Geology (2020), vol. 114, 104203. DOI: https://doi.org/10.1016/j.marpetgeo.2019.104203. This is an author version of the article. For the final copy-edited version, please visit: https://www.sciencedirect.com/science/article/pii/S0264817219306579

1. Introduction

Carbonate reservoirs are notoriously complex to develop for hydrocarbon production due to strong spatial and temporal variations in petrophysical properties which, when combined with the presence of sub seismic-scale structures, inevitably impact reservoir quality (*e.g.*, Agar and Geiger, 2015). Sub-seismic-scale structures in carbonate rocks, such as fractures and stylolites, can have profound impacts on the bulk rock permeability and fluid flow pathways (Burgess and Peter, 1985; Guerriero *et al*., 2013; Larsen *et al*., 2010), requiring the use of predictive guides to help understand their influence. Previous work on the characterisation of sub seismic-scale structures in carbonate reservoirs that influence fluid flow has mostly focused on fracture networks (*e.g.*, Long and Witherspoon, 1985; Nelson, 2001; Di-Cuia *et al.*, 2005; Guerriero *et al*., 2013; Haines *et al*., 2016). Identifying the sedimentological and diagenetic controls on mechanical stratigraphy (Laubach *et al.*, 2009) enables predictions to be made about fracture distribution based on lithofacies.

Stylolites are irregular dissolution surfaces with multiscale roughness created by intergranular pressure solution (Koehn *et al*. 2007; Ebner *et al.* 2010). These dissolution seams are primarily associated with strain localisation and form thin lateral drapes (Heap *et al*. 2014), which commonly host relatively insoluble particles such as clay minerals, oxides, organic matter, etc. (Nelson, 1981; Railsback, 1993; Ben-Itzhak *et al*., 2014). High solubility and fast reaction kinetics make carbonate rocks the predominant lithology susceptible to pressure-solution, although stylolites have been found to develop in sandstones (Baron and Parnell, 2007; Nenna and Aydin, 2011), evaporites (Bäuerle *et al*., 2000) and other rock types. Along with sub-seismic-scale fractures, understanding the controls on stylolite network distribution is hampered by the high reactivity and complex mechanical behaviour of carbonates (Fabricius, 2014). Stylolites can control petrophysical properties and fluid flow in different ways (*e.g.*, Paganoni *et al*., 2016; Martín-Martín *et al*., 2017; Heap *et al.*, 2018; Toussaint *et al.*, 2018; Bruna *et al.*, 2019). However, despite their abundance in carbonate rocks, less attention has been paid to their study compared to fracture networks.

Stylolite morphologies and their orientation can be used to unravel the orientation and magnitude of principal compressive stress in an area (Koehn *et al.*, 2012). Bedding-parallel stylolites form during vertical sediment compression due to compaction associated with burial. The morphology of stylolites varies greatly according to their amplitude, wavelength, spacing and connectivity, producing a variety of stylolite network geometries (Vandeginste and John, 2013; Ben-Itzhak *et al*., 2014). Stylolite networks have been predominantly studied in association with their influence on fluid flow, since stylolites have demonstrated a range of behaviours when interacting with fluids. Some studies suggest that stylolites can act as baffles to fluid flow (*e.g.*, Burgess and Peter, 1985; Finkel and Wilkinson, 1990; Dawson, 1998; Alsharhan and Sadd, 2000; Gomez-Rivas *et al.*, 2015; Martín-Martín et al., 2017) based on field and petrographic observations. Alternatively, stylolites have been found to act as conduits that improve permeability along their orientation as observed in some carbonate reservoirs and outcrops (*e.g.*, Carozzi and Bergen 1987; Bergen and Carozzi, 1990; Lind *et al.*, 1994; Harris, 2006; Chandra *et al*., 2014; Barnett *et al.*, 2015; Paganoni *et al.*, 2016; Martín-Martín *et al.*, 2017; Morad *et al.*, 2018) in addition to laboratory permeability tests (*e.g.*, Heap *et al*., 2014, 2018; Rustichelli *et al*., 2015). The development of localised porosity around stylolites has been associated with preferential dissolution along existing stylolite planes (Bergen and Carozzi, 1990) and an increase in the average size of pore throats (Baud *et al*., 2016).

The influence of fluids on the development and effect of stylolites is also uncertain. Petroleum emplacement may inhibit stylolitisation (*e.g.*, Neilson *et al*., 1998; Morad *et al.*, 2018). Laterally extensive stylolite networks, however, are present in hydrocarbon-bearing limestones and can compartmentalise reservoirs causing variations in fluid flow (Hassan and Wada, 1981; Ehrenberg *et al*., 2016). The scale of impact is also an important concept. Heap *et al*. (2014) suggests that the discontinuous nature of stylolites only affects petrophysical properties on a local scale. They (ibid.) suggest that stylolitic porosity creates elongated 'finger-like' pores aligned with stylolite teeth and larger pore throat radii along fluid flow paths that are parallel to stylolites. Heap et al. (2018) also indicate that stylolites can cause permeability anisotropy, where permeability is higher along the stylolite surface.

Whilst the role of stylolites on fluid flow at the local scale has been extensively studied and remains a controversial topic, there is still uncertainty as to how sedimentary facies and carbonate rock components influence stylolite morphology, type and growth. Along with this there has been a growing interest for understanding the role of host rock heterogeneity on stylolite morphology, location and extent (Toussaint *et al*., 2018; Morad *et al.*, 2018). Whilst previous authors identify key lithological controls on stylolitisation, Koehn et al. (2016) highlight the importance of how these lithological controls interact with each other to impact stylolite formation.

The complex nature of stylolites has led to an array of literature covering a range of topics associated with stylolite formation, morphology, distribution and influences on fluid flow and mechanical strength (*e.g.*, Andrews and Railsback, 1997; Aharonov and Katsman, 2009; Koehn *et al*., 2012; Baud *et al*., 2016; Koehn *et al*., 2016; Toussaint *et al*., 2018; Heap *et al*., 2018). However, the diverse focus on different facets of stylolite behaviour has subsequently led to the absence of a comprehensive established methodology for the collection of outcrop-scale stylolite measurements.

This study aims to statistically characterise stylolite morphology and distribution in different platform carbonates, based on outcrop-scale observations of the Aptian-Albian Benassal Fm exposed in the Benicàssim half graben (Maestrat Basin, Spain) (Fig. 1). The specific objectives are: i) to identify sedimentary stylolite populations and quantify their properties (type, density, amplitude and connectivity) in seven typical Early Cretaceous shallow marine lithofacies, including dolostones (Fig. 2), which crop out in the Orpesa Range; ii) to statistically analyse the collected data sets to infer relationships between stylolite properties and lithofacies characteristics; and iii) to discuss the most important lithological influences on stylolite morphology and distribution. This well-studied area allows multiple stylolite populations to be sampled in outcrops that have undergone very similar and well-known burial histories, removing the influence of stress variations and instead allowing observations to be directly related to lithofacies and diagenetic textures formed prior to chemical compaction. The results of this study provide an estimation of pressure-solution signatures of typical platform carbonate lithofacies, helping to predict the presence and properties of stylolites when limited subsurface data are available.

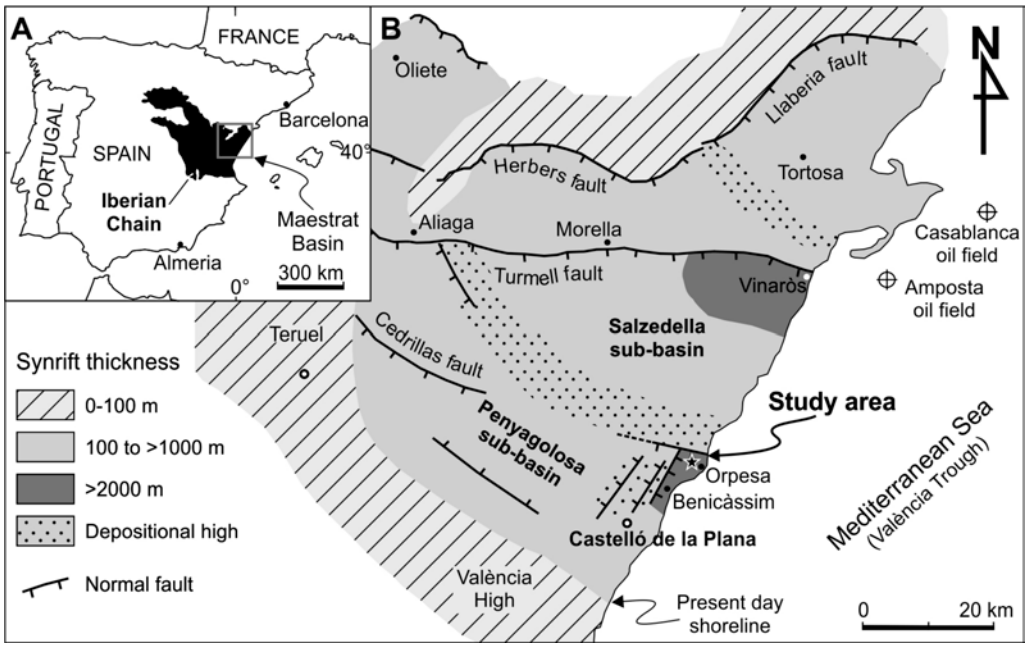

Fig. 1. (A) Simplified map of the Iberian Peninsula showing the location the Maestrat Basin in the Iberian Chain (square). (B) Paleogeographic map of the Maestrat Basin showing the thickness distribution of Late Jurassic-Early Cretaceous succession along the basin. Key sub-basins are labelled as Morella (Mo), Salzedella (So), Penyagolosa (Pe), Oliete (Ol) and Galve (Ga). The star represents the location of the main study area relative to Benicàssim and Orpesa. Key sampling location coordinates in this study are 40.110413° N, 0.123381° W and 40.111254° N, 0.125295° W. Modified after Salas et al. (2001) and Martín-Martín et al. (2017).

2. Geological setting

2.1. Structure and stratigraphic architecture of the Benicàssim area

The Maestrat Basin is located in the east margin of the Iberian Chain, formed by the Mesozoic inversion of the intraplate Iberian Rift System (Salas *et al*., 2001). Two main cycles of syn- and post-rifting occurred between the Late Triassic and Late Cretaceous, of which the second rift cycle was responsible for the breakup of the Iberian Basin and the formation of the Maestrat basin (Salas and Casas, 1993; Salas *et al*., 2001; Nebot and Guimerà, 2016). According to these authors, the Maestrat Basin was compartmentalised into several sub-basins (Salas and Guimerà, 1996) and is bound to the north and south by listric extensional faults (Nebot and Guimerà, 2016). Inversion associated with the Alpine Orogeny in the Eocene to Early Miocene led to uplift of the Maestrat Basin (Liesa *et al*., 2006; Nebot and Guimerà, 2016). Neogene extension opened the Valencia Trough on the present-day eastern margin of the Maestrat Basin (Salas *et al*., 2001), which also partly reactivated Cretaceous extensional features on the eastern part of the Iberian Chain (Guimerà *et al*., 2004).

The Late Aptian and Early Albian Benassal Fm was deposited during the second rift cycle of the Maestrat Basin. Strong subsidence during rifting facilitated syn-rift deposition of Early Cretaceous carbonates in excess of 2 km thick, resulting in the deposition of the Benassal Fm with a present-day thickness of at least 1,600 m (Yao, 2019). Depositional facies are characterised by abundant rudists, corals and orbitolinids, signifying an evolution

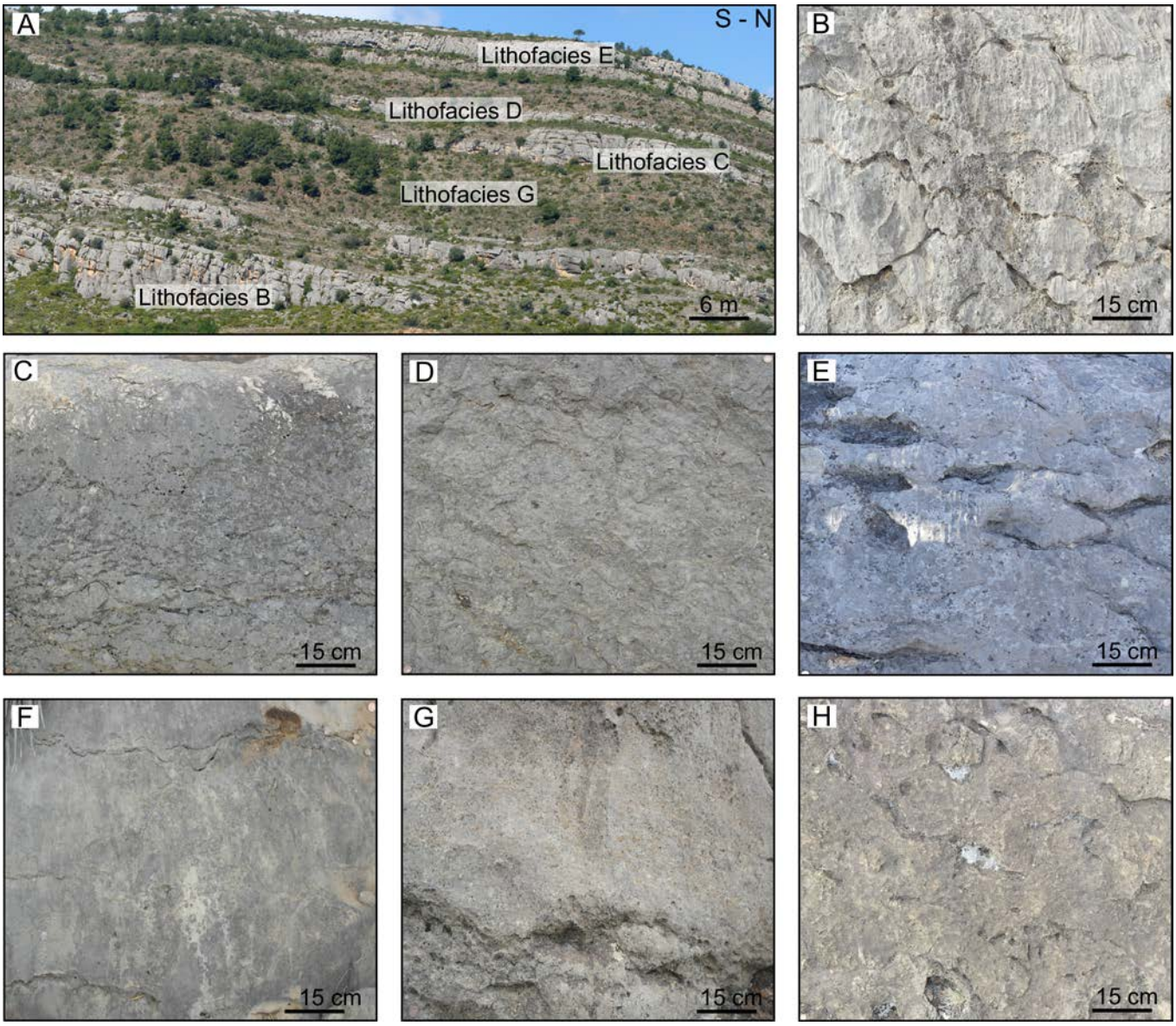

Fig. 2. (A) Panoramic photograph of the Benassal Fm. Photo plates of studied lithofacies in order of high to low energy; spicule wackestone (B), bioclastic wackestone/packstone (C), rudist floatstone (D), coralline limestone (E), ooidal/peloidal grainstone (F), bioclastic grainstone (G) and dolostone (H).

from basinal to inner-ramp settings on a shallow-marine carbonate ramp (Martín-Martín *et al*., 2013; Yao, 2019). The Benicàssim half graben is defined by two Early Cretaceous large-scale faults, inherited from the Variscan orogeny: the NNE-SSW striking Benicàssim Fault, and the E-W striking Campello Fault (Martín-Martín *et al*., 2013; Martín-Martín *et al*., 2015; Yao, 2019). These faults were also re-activated during the Alpine orogeny and the Neogene extension periods (Gomez-Rivas *et al.*, 2012). The Benassal Fm is partially dolomitised and hosts Mississippi Valley-type (MVT) mineral deposits (Corbella *et al*., 2014; Gomez-Rivas *et al*., 2014). Dolomitised geobodies range from massive patches next to fault zones to connected stratabound geometries that extend for several kilometres away from them (Martín-Martín *et al*., 2013; Corbella *et al*., 2014; Gomez-Rivas *et al*., 2014; Martín-Martín *et al*., 2017; Yao, 2019). Dolomitisation occurred between 400-700 m burial depths and predominantly replaced grain-supported lithofacies and beds located between strongly stylolitised limestone facies (Martín-Martín *et al*., 2015). Chemical compaction (*i.e.*,

stylolitisation) predated dolomitisation, and was estimated to have taken place at relatively shallow burial depths between 300-800m (Martín-Martín *et al*., 2017). Additional diagenetic processes postdating both stylolitisation and dolomitisation included cementation by saddle dolomite, and burial and meteoric calcite, as well as calcitisation of replacive and saddle dolomites (for a complete review of the paragenesis see Martín-Martín *et al*., 2015).

2.2. Lithofacies

According to Martín-Martín et al. (2013) and Yao (2019), the Benassal Fm carbonates of the Orpesa Range can be subdivided into 15 lithofacies and are stacked into three transgressive-regressive sequences (I, II, III). Sequence I contains transgressive deposits of green basinal marls containing brachiopods and echinoderms, interbedded between cross-bedded peloidal and orbitolinid grainstones. These are overlain by regressive peloidal grainstones, orbitolinid wackestones to rudstones and coralline limestones that are topped by a thick package of rudist floatstones. Sequence II begins with transgressive tidally influenced grainstones, overlain by sponge spicule wackestones. Regressive lithofacies initiate with coralline limestones and orbitolinid wackestones that are capped by grainstones with hummocky-cross stratification, bioclastic wackestones and packstones and peloidal grainstones. Sequence II is also topped by a thick unit of rudist floatstones representing the most regressive deposits. Sequence III has transgressive bioclastic wackestones and packstones, which are overlain by a thick dolostone unit with internal limestone stringers. Above the dolostone are regressive ooidal grainstones, bioclastic wackestones and packstones, peloidal grainstones, finally topped by another dolostone unit.

3. Methods

A variety of stylolite measurements were performed in all lithofacies in order to characterise stylolite network morphologies. Outcrop-scale measurements were collected from field observations using the previously defined lithofacies by Martín-Martín et al. (2013) and Yao (2019) in the Orpesa Range to statistically characterise stylolite populations. These lithofacies include (in order of potential mechanical strength): spicule wackestone (A), bioclastic wackestone/packstone (B), rudist floatstone (C), coralline limestone (D), ooidal/peloidal grainstone (E), bioclastic grainstone (F) and dolostone (G). Lithofacies were sampled using optical petrography to determine rock texture, facies and components. Sampling windows with an area of 1 m^2 were used to measure the density, type and size of stylolites in different lithofacies, where windows were positioned adjacently along stratigraphic beds to mitigate against vertical lithological changes. Windows were created at the outcrop using markers which allowed them to maintain the same dimensions and scale when being photographed, regardless of camera zoom and positioning. Stylolite spacing measurements (Fig. 3) were collected in-situ whilst other parameters, such as stylolite connection angles and intersection types, were collected from scaled window photographs. Using vector graphics software, stylolites were traced in black and shown on a white background for each window photograph, to reduce the impacts of vegetation/background noise on stylolite data collection. As a result of photograph resolution limitations and subsequent truncation bias (Zeeb *et al*., 2013), stylolite seam measurements typically between 3 – 7 pixels were sampled. All spatial measurements (*i.e.*, stylolite spacing, amplitude and wavelength) were measured from photographs in pixels and subsequently converted into centimetres using a conversion ratio defined by the sampling window.

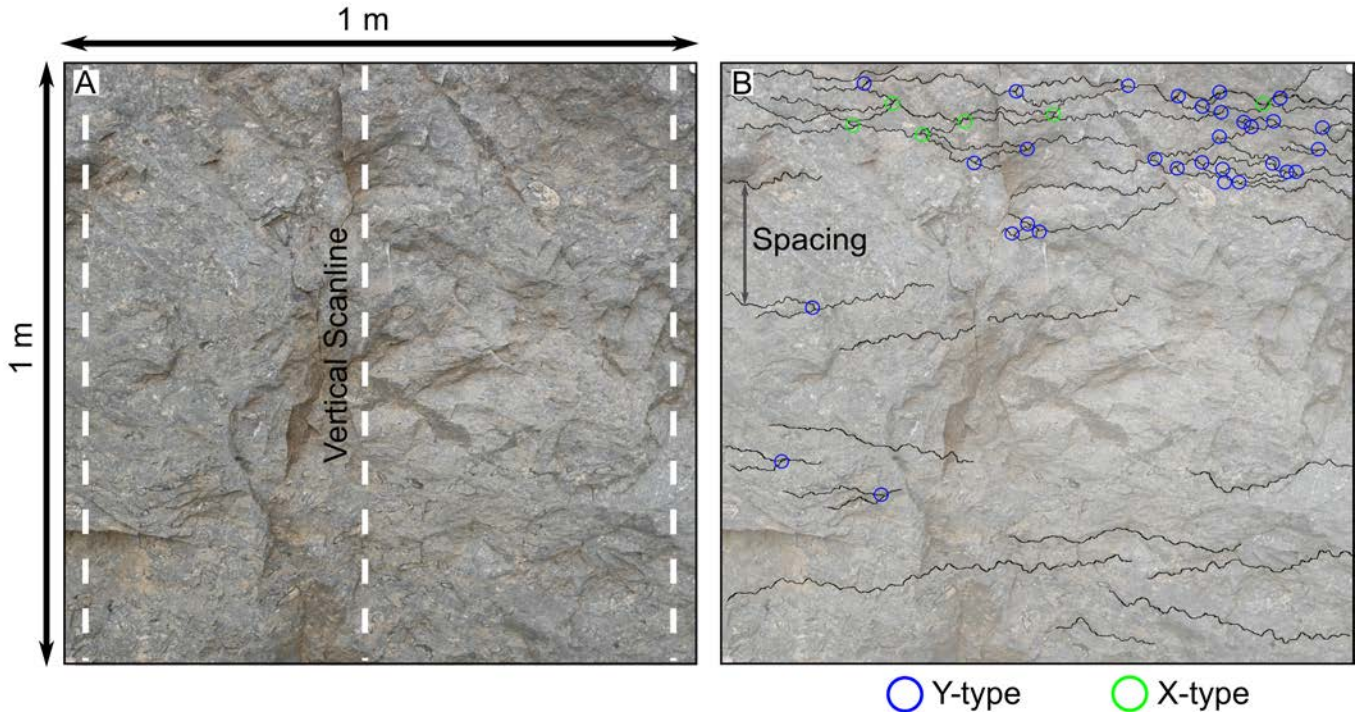

Fig. 3. (A) Example of sample window dimensions and locations of three scanlines used for sampling stylolite spacing measurements. (B) Annotated photograph categorising stylolite intersection type as either X-type or Y-type.

To measure stylolite spacing, three 1 m-length vertical scanlines, with a horizontal offset of 50 cm, were created in each 1 m^2 sampling window (Fig. 3). Scanlines were drawn perpendicular to stylolites to avoid orientation bias. The vertical distances between stylolites intersecting each scanline were recorded in the field using a tape measure, with vertical spacing measurements from each scanline being totalled per window (Fig. 3). The detection limit, *i.e.* the maximum vertical stylolite spacing measurement able to be recorded, is one metre, as it is determined by the height of the field-sampling window. However, it is worth noting that the spacing in all the facies analysed was always significantly lower than 1 m, validating the size of the sampling window used here.

Stylolite wavelength and amplitude measurements were collected using a single vertical scanline situated in the middle of the sampling window. All stylolites that intersected the scanline were measured. Wavelength was recorded as the horizontal distance between the nearest peak-peak or trough-trough that was situated on the scanline, whilst amplitude measurements were represented by the vertical height of a stylolite tooth on or closest to the scanline (Fig. 4a, b). Collecting the closest amplitude measurements to the scanline reduced size bias, although censorship bias limited measurements greater than the 1 m-wide sampling window from being recorded.

Distribution fitting was carried out on stylolite spacing, wavelength and amplitude measurements from each lithofacies to assess which statistical distribution represented each dataset. Stylolite data were fitted to three common statistical distributions – exponential, power-law and log-normal. The quality of the fits was evaluated using a chi-squared test alongside a Kolmogorov-Smirnoff (KS) normality test (Massey, 1951). Higher chi-squared values indicate a higher goodness of fit between the fitted distributions and stylolite dataset. For KS test results the null hypothesis is that stylolites do not fit the distribution being

assessed and therefore have a less than 0.05 p-value, whereas a p-value greater than 0.05 suggests that stylolite measurements are best represented by the assessed distribution and therefore the null hypothesis is rejected. Histograms of stylolite of the 10-based logarithm of spacing, wavelength and amplitude were constructed with the open-source software Past 3.11 (Hammer *et al*., 2001). Each dataset is divided in 20 equal-width bins, spanning the range of the set. Different distributions are fitted to each dataset, including a normal distribution fitted to each distribution of the log of the values. The goodness of fit is reported as the correlation coefficient (*r*) of a straight line in the normal probability plot.

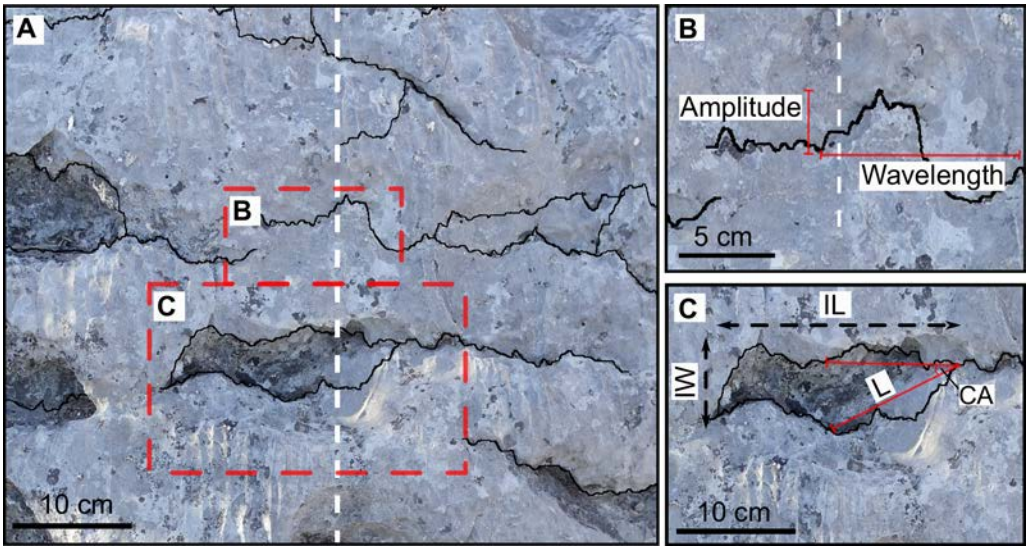

Fig. 4. (A) Annotated field image of a sampling window with scanline used for stylolite wavelength and amplitude measurements. (B) Example measurements for stylolite wavelength (W) and amplitude (A). (C) Example of collection stylolite island dimensions (IL & IW) and connection angle (CA) measured as a function of length (L) using methodology by Ben-Itzhak *et al*. (2014).

Stylolite populations were identified by Ben-Itzhak *et al*. (2014) as forming a range of geometries based on the connectivity of stylolites, defined as isolated, long-parallel and anastomosing. Measuring the angle of connectivity in stylolite populations has been suggested as a method to understand whether anastomosing networks form through the connection of isolated stylolites by cannibalisation, where individual stylolites roughen and merge together (Ben-Itzhak *et al*., 2014). The dimensions of 'islands' or 'lenses', the length and height of rock space situated between anastomosing stylolites, can allow estimating the amount of dissolution required in order to generate anastomosing populations (Ben-Itzhak *et al*., 2014) and measuring the intensity of anastomosis.

Connectivity measurements were recorded for anastomosing stylolite networks in only four lithofacies in which these geometries were present (coralline limestone, bioclastic wacke/packstone, rudist floatstone and spicule wackestone) using the method defined by Ben-Itzhak *et al*. (2014). Measurements investigating connectivity focused on two aspects based on the dimensions of the area between stylolites and the angle of stylolite junctions (Fig. 4a, c). The dimensions of stylolite 'islands' (IL and IW for island length and width, respectively) were acquired to provide a distribution of areal measurements and length to width ratios that were examined per window and totalled for each lithofacies to provide a distribution of 'island' dimensions. Stylolite islands were assumed to be rectangular when measuring IL and IW (Fig. 4c). Connection angles (CA) were measured at stylolite junctions,

where the angle between two stylolites was recorded at different lengths (L), or distance, measured from the stylolite intersection point. Angles were recorded at 1 cm intervals from stylolite intersections to provide a distribution of connection angles per lithofacies. The maximum distance which stylolite intersection angles were measured was defined as the midpoint of a stylolite 'island' with anastomosing stylolites, or the ends of stylolites that were laterally discontinuous.

The density of stylolite intersection types were measured as a function of stylolite length. Intersections were classified, based on the scheme by Manzocchi (2002) and Sanderson et al. (2015) used for fracture network connectivity, as either X or Y (Fig. 5). To calculate the density of intersections per facies, the total number of intersections per window was divided by the total horizontal stylolite length per window. This provided a ratio of stylolite intersection density per metre (/m) for each window, which was then averaged to provide a ratio for each lithofacies (Eqn. 1):

$$\text{ID (/m)} = (I_{wn} / (SL_{wn}) \quad \text{(Eqn. 1)}$$

Where ID (/m) is the intersection density per metre, I_{wn} is the total number of intersections per sampling window, and SL_{wn} is the total stylolite length per window measured in pixels. The total stylolite length per sampling window (SL_{wn}) is affected by the size of the sampling window and therefore is not representative of the actual horizontal length of stylolite networks, but it is useful for normalising intersection density for each sampling window in order to compare densities between lithofacies.

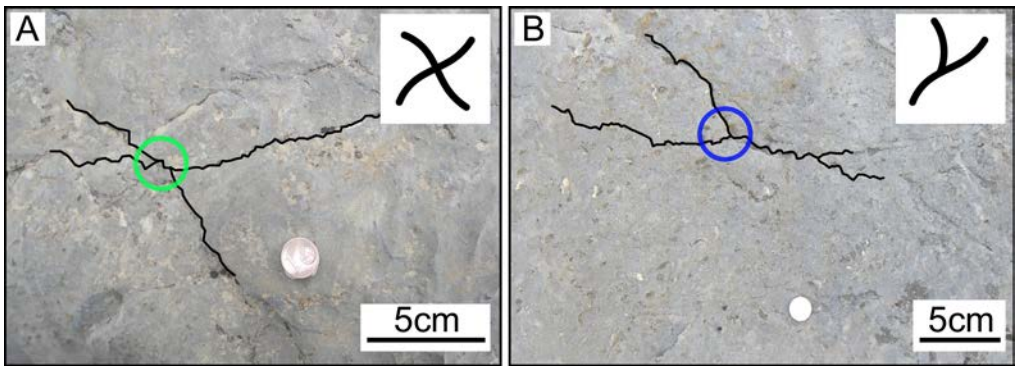

Fig. 5. Annotated field image showing stylolite intersection types. (A) X-type. (B) Y-type.

Stylolites in each photograph were classified based on morphology using definitions by Koehn *et al.* (2016), where stylolites are classified as rectangular layer type, seismogram pinning type, suture and sharp-peak type, and wave-like type (for an overview of stylolite morphologies see Koehn *et al.*, 2016 and Humphrey *et al.*, 2019). Stylolite types were counted per window and totalled to obtain the relative frequencies of stylolite types per lithofacies.

Whilst Ben-Itzhak et al. (2014) devised techniques suited for evaluating stylolite connectivity, our current sampling techniques are based on methods used for fracture network characterisation and inadvertently contain one or more sampling biases which are orientation-, censorship- (*i.e.*, altering sampling area boundaries) or truncation-related (see discussion by Zeeb *et al.*, 2013 for fracture network analysis). Because of this, a combination of measurement methods is required to effectively characterise stylolite networks whilst

mitigating against bias. Collecting measurements using vertical scanlines, orientation bias may underestimate vertical stylolite spacings by failing to record oblique stylolites that did not intersect the scanline. However, as the vast majority of stylolites in this study are bedding-parallel, orientation bias is not significant. Censorship bias affects the coverage of the sampling area as a result of vegetation or outcrop exposure, typically leading to the overestimation of density measurements (at least in fracture networks) (Zeeb *et al*., 2013). Whilst exposure in each sampling area did vary, sampling windows used for collecting stylolite measurements were positioned adjacently and, where possible, at fixed intervals to improve the coverage of sampling and mitigate against measurements being collected from exclusively well-exposed areas with dense stylolite populations. The relationship between stylolite morphology measurements and the sedimentological properties of sampled lithofacies was assessed by using a correlation matrix. Categorical variables (*i.e.*, degree of sorting) were firstly converted into a numerical format and the Pearson correlation coefficient was calculated for each pair of input parameters (both stylolite measurements and sedimentological properties). Correlation coefficients ranged between -1 and +1 to indicate negative and positive correlations respectively.

4. Results

4.1. Definition of lithofacies

This section describes the texture characteristics of the seven lithofacies to highlight potential features that can potentially be correlated with stylolite properties (Fig. 2).

Spicule wackestone (*Facies A*) is composed of a micritic matrix that shows poor-moderate sorting with less than 10% of grains larger than 2 mm, with minimal bioclasts (bivalve fragments and foraminifera) (Fig. 6a, b). Calcitised spicules are evenly distributed throughout the matrix and are randomly orientated (Fig. 6a, b). Spicule wackestone has metric-scale bedding with minimal vertical fracturing.

Bioclastic wackestone/packstone *(Facies B)* has a poorly sorted micritic matrix with less than 10% of grains larger than 2 mm. Bioclastic wackestone and packstone are arranged in alternating layers with abundant bioclasts. Primary grain components are orbitolinids, *Chondrodonta* bivalve, miliolids and other foraminifera (Fig. 6c, d), whilst secondary components include peloids, spicules and echinoderm fragments (Fig. 6d). Small fractures appear partially cemented by calcite (Fig. 6c). Bioclastic wackestone/packstone has decimetre-scale bedding.

Rudist floatstone *(Facies C)* is made of a micritic matrix with more than 10% of grains larger than 2 mm. Primary bioclasts are rudists, which remain predominantly intact, alongside poorly sorted orbitolinids, miliolids and bivalve fragments (Fig. 6e). Minor quantities of echinoderm fragments are present and have been subject to micritisation (Fig. 6e), whilst rudist fragments are calcitised (Fig. 6f). Rudist fossils remain intact with a diameter of 3-4 cm however some fossils can be >10 cm diameter. Rudist floatstone has metric-scale bedding that is well exposed in outcrop.

Coralline limestone *(Facies D)* has a micritic texture with less than 10% of components exceeding 2mm. Primary skeletal components consist of coral and bivalve fragments, both of which have been replaced by calcite (Fig. 7a). The original structure of

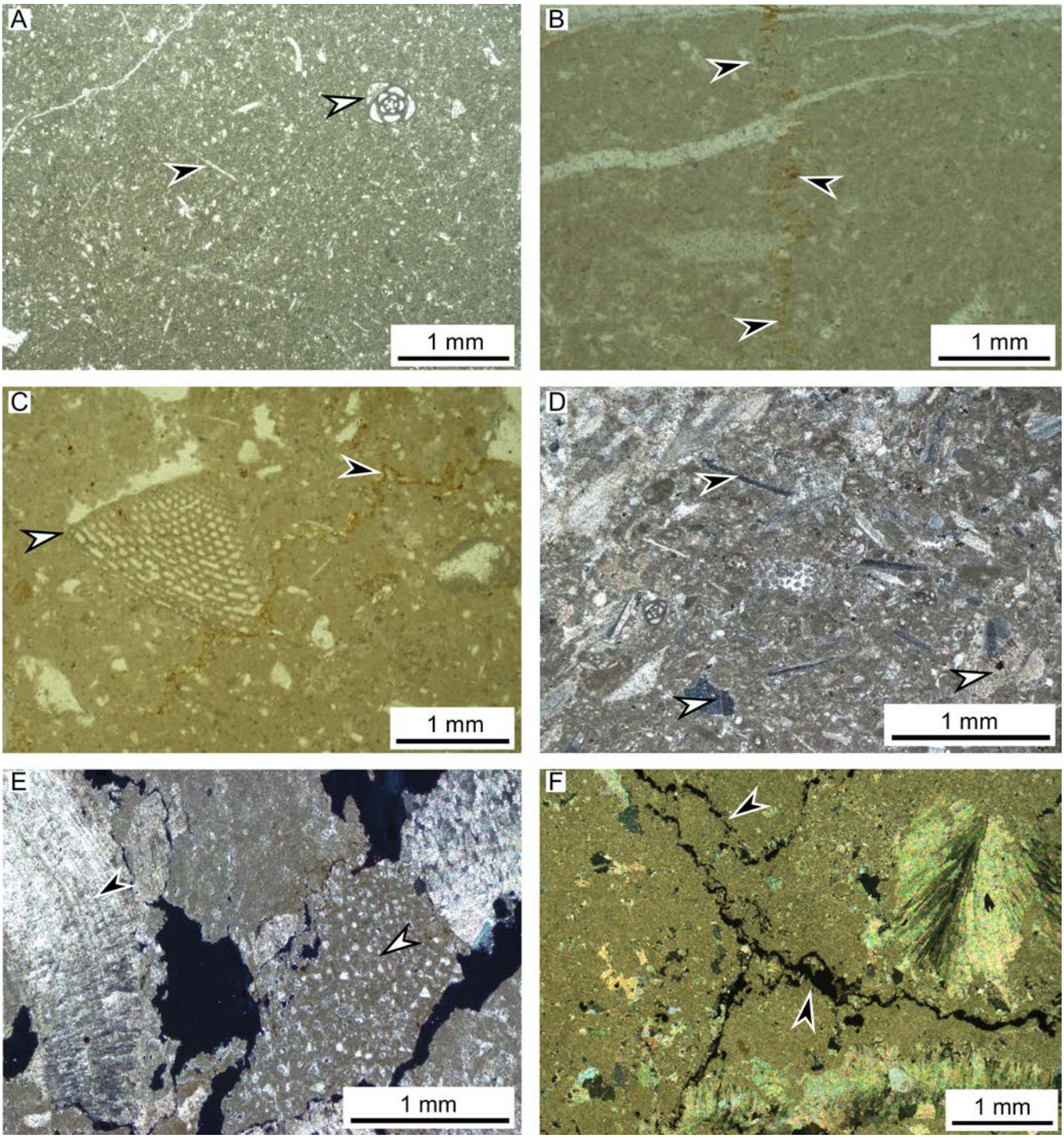

Fig. 6. Photomicrographs showing textural characteristics of lithofacies. (A) Spicule wackestone (plane polarised light; PPL) with sponge spicules (black arrow) distributed in a mass made of fine-grained skeletals and micrite alongside with minor foraminifera (white arrow). (B) Spicule wackestone (diffused light; DL) with a weakly defined stylolite (black arrows) that shows weak iron staining. (C) Bioclastic wackestone/packstone (DL) with orbitolinid (white arrow) and stylolite (white arrow). (D) Bioclastic wackestone/packstone (cross polarised light; XPL) with abundant bivalve fragments (black arrow) and a minor quantity of echinoderm fragments (white arrows). (E) Rudist floatstone with preserved growth laminations (black arrow) and an orbitolinid fragment (white arrow). (F) Rudist floatstone with open anastomosing stylolites (black arrows) propagating along grain-matrix contact.

bivalves is preserved (Fig. 7b). Minor quantities of peloids are distributed throughout the matrix and show no evidence of preserved internal structures. The distribution of primary and secondary components indicates a poor degree of sorting. Fine fractures cemented by calcite crosscut all components (Fig. 7b). Coralline limestone has metric-scale bedding with a weathered nodular appearance.

Ooidal/peloidal grainstone *(Facies E)* has a well sorted, grain-supported texture with less than 10% of grains exceeding 2 mm in size. Grains are evenly distributed with no apparent clustering or compaction of grains (Fig. 7c, d). Ooids and peloids are the primary lithofacies components, with their relative abundance varying slightly across the sample to produce marginally more ooid/peloid-rich areas. Ooids have poorly developed concentric cortices (Fig. 7c, d), whilst peloids appear to have weakly defined internal structures. Bioclasts present include miliolids and echinoderm fragments (Fig. 7d). There is a higher proportion of calcite cement between bioclasts relative to the bioclastic grainstone lithofacies. Ooidal/peloidal grainstone beds typically have centimetre-scale thicknesses.

Bioclastic grainstone *(Facies F)* has a well-sorted, grain-supported texture with more than 10% of components larger than 2 mm. There is a high density of peloids and bioclasts, occasionally causing grainstones to be classified as peloidal rather than bioclastic, where some areas feature grains that are compacted (Fig. 7e). Skeletal components are predominantly *Chondrodonta* bivalves, which are vertically orientated in life position, alongside rudists that have an approximate diameter of 10 cm. Orbitolinids, miliolids and bioclastic fragments also occur in minor abundance. Intraclasts and abundant peloids are also present. Fractures cemented by calcite crosscut the rock components (Fig. 7e). Approximately 10-15% of micritised grains have yellow discolouration from iron staining. Grainstones form decimetric- to metric-scale beds that are vertically fractured.

Dolostone *(Facies G)* comprises dolomite crystals with a planar-e to planar-s texture, with some crystals being planar-anhedral (Fig. 7f). According to the detailed petrographic analysis by Martín-Martín et al. (2015) and Martín-Martín et al. (2017), bedding-parallel stylolites predate dolomitization in this area. However, stylolites were only occasionally preserved (Fig. 7f) during dolomitisation and are therefore not widespread. Dolostone is well exposed in outcrop and consists of metric-scale beds.

4.2. General characteristics of stylolite networks for each lithofacies

Stylolites in spicule wackestone (Facies A) (Fig. 8a) are well exposed with minor weathering and are found to be evenly distributed throughout beds regardless of proximity to bedding surfaces. Stylolite morphology is dominantly suture and sharp-peak type with occasional wave-like type stylolites, which connect with each other both laterally and vertically to create anastomosing networks. Stylolite intersections are typically Y-type and therefore stylolite networks have a branching appearance.

Bioclastic wackestone/packstone (Facies B) (Fig. 8b) stylolites have a similar outcrop appearance as spicule wackestone (Facies A), however the stylolites are less weathered and harder to trace laterally. Stylolites are evenly distributed throughout beds and have a suture and sharp-peak type morphology with minor occurrences of wavy- and rectangular layer type morphologies. Stylolite networks appear isolated and laterally discontinuous in outcrop however occasionally stylolite networks anastomose, producing Y- and X-type intersections.

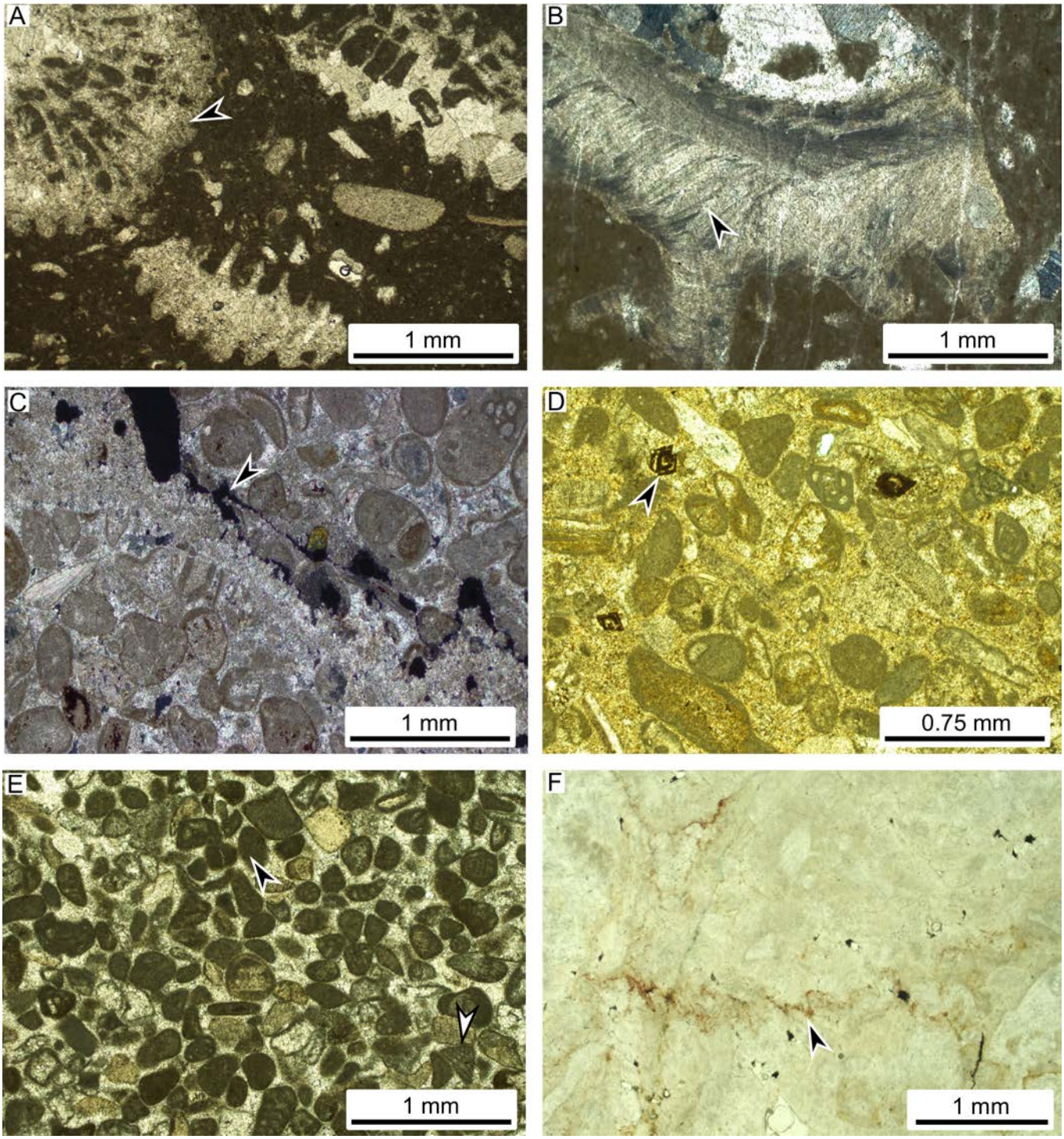

Fig. 7. Photomicrographs showing textural characteristics of lithofacies. (A) Coralline limestone (PPL) showing fragments of corals within the micritic matrix (black arrow). (B) Coralline limestone (XPL) with a bivalve fragment showing preserved growth laminations (black arrow). (C) Ooidal/peloidal grainstone (XPL) with stylolite showing minor anastomosis (black arrow). (D) Ooidal/peloids grainstone (PPL) with a minor quantity of dolomite rhombs (black arrow). (E) Peloidal grainstone (PPL) with abundant peloids (black arrow) and benthic foraminifera (white arrow). (F) Crystalline dolomite texture (DL) with remnant of a stylolite (black arrow).

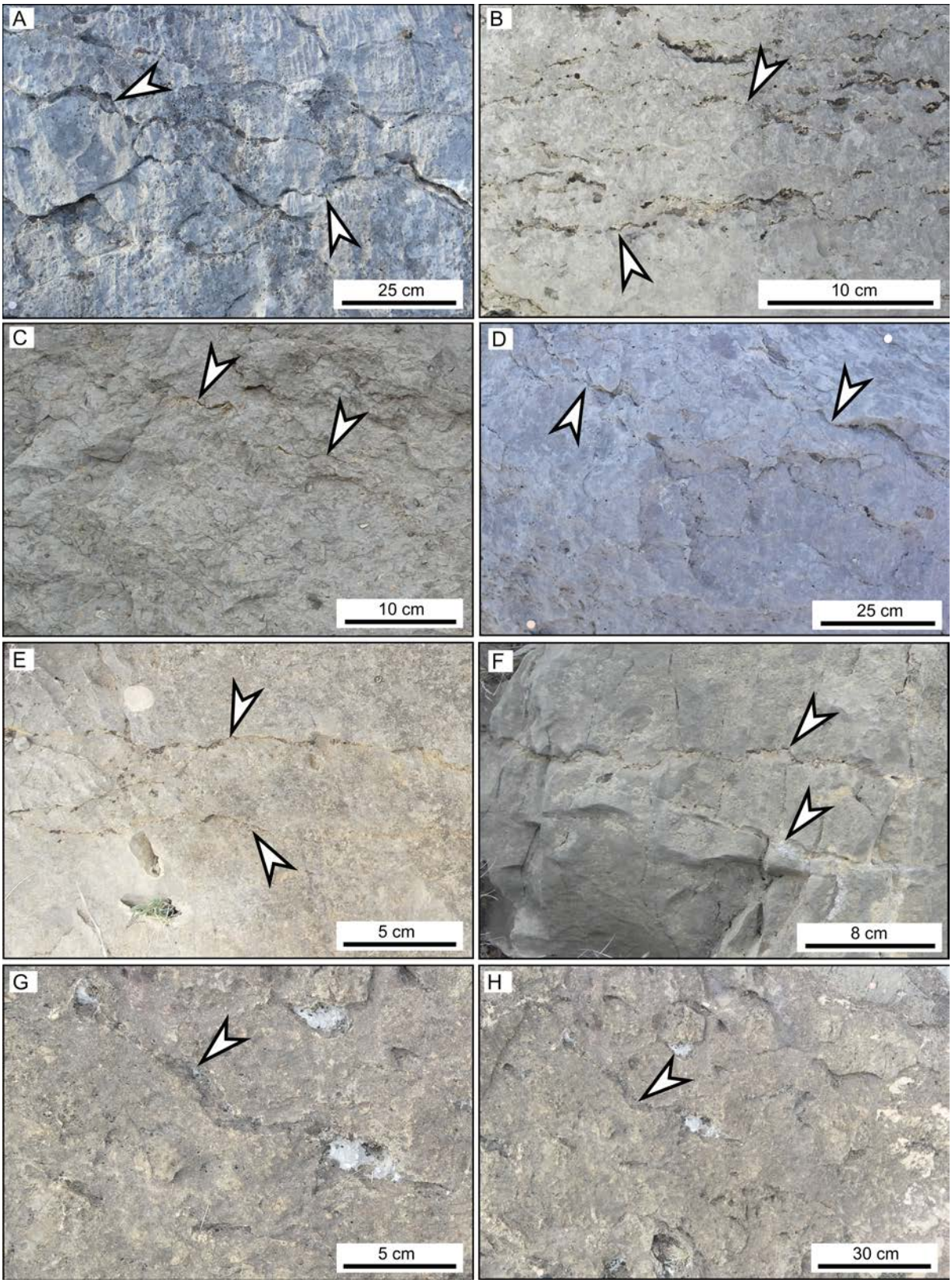

Fig. 8. Photo plate of stylolite network morphologies in sampled lithofacies with annotated stylolites (white arrows). (A) Spicule wackestone. (B) Bioclastic wackestone/packstone. (C) Rudist floatstone. (D) Coralline limestone. (E) Ooidal/peloidal grainstone. (F) Bioclastic grainstone. (G) Dolostone. (H) Dolostone.

Stylolites are well developed in rudist floatstone (Facies C) (Fig. 8c) samples and distributed mostly along the grain-matrix contact, but also within the micritic matrix. Suture and sharp-peak type morphology is dominant with minor occurrences of wave-like type stylolites. Stylolites show evidence of anastomosis, with stylolite convergence typically along the grain-matrix contact where rudists are present. Y-type intersections are common, with a minor abundance of X-type intersections.

Stylolites in coralline limestone (Facies D) (Fig. 8d) have been weathered but can be distinguished on the surface of outcrops. Stylolites are preserved and nucleate within the matrix. However, stylolite interaction with grains/mineralogical contrasts is low as calcitised grains are sparse (Fig. 6f). Stylolites are a dark yellow colour from iron staining. Stylolite morphology is dominantly suture and sharp-peak type stylolites with occasional wave-like type stylolites which can be observed as both anastomosing and forming long parallel networks.

Stylolites in ooidal/peloidal grainstone (Facies E) (Fig. 8e) lithofacies are easy to distinguish in outcrop due to extensive weathering and appear to develop along bedding surfaces, whilst some beds display weak cross bedding. Similar to other lithofacies, suture and sharp-peak type as well as wave-like type stylolites are the dominant stylolite morphology although ooidal/peloidal grainstone contains a larger relative abundance of rectangular layer type stylolites compared to all other studied lithofacies. Stylolites appear laterally discontinuous and form isolated networks.

Bioclastic grainstone (Facies F) (Fig. 8f) have stylolites with similar outcrop exposure to ooidal/peloidal grainstone (Facies E), where stylolites also develop proximal to bedding surfaces. Stylolite morphologies are suture and sharp-peak type and wave-like type, which appear to have similar relative abundances, alongside a minor abundance of rectangular layer type stylolites. Stylolites terminate laterally and are isolated with minimal vertical connectivity.

Dolostone (Facies G) (Fig. 8g, h) have stylolite populations that were difficult to observe due to outcrop weathering associated with calcitisation and meteoric alteration of the rock. Calcite and saddle dolomite precipitated in vugs which are often located parallel to stylolite orientations. Stylolites have similar abundances and distributions to studied grainstone lithofacies (Facies E and F), with suture and sharp-peak type and wave-like type morphologies. Stylolites are isolated and have long-parallel geometries.

4.3. Stylolite statistical properties

Stylolite populations were initially characterised through outcrop-scale measurements to define statistical properties of stylolite morphology within each studied lithofacies. Morphological properties used to statistically characterise stylolites consisted of vertical spacing, amplitude, wavelength, intersection type and intersection density (Table 1).

Bioclastic wackestone/packstone has the smallest vertical stylolite spacings, where 50% of spacings are between 0-5 cm and 38% of spacings are between 6-12 cm when measured in 1 m^2 sampling windows (Fig. 9). Comparatively, dolostones have the largest spacing, with 50% of measurements progressively increasing from 17 to 61 cm. A small proportion of spacing measurements (cumulative frequency of 15%) in ooidal/peloidal grainstone are of a similar size from 31-58 cm, as in the dolostones. Most of the spacing sizes

between stylolites in ooidal/peloidal grainstones (cumulative frequency of 55%) range from 10 to 29 cm below which the spacings converge with the majority of the remaining lithofacies. All other lithofacies have similar spacing frequencies, with 50% of measurements approximately between 0 and 12 cm. In these, the distribution of spacing measurements from 6 to 51 cm varies. Bioclastic grainstone, spicule wackestone and coralline limestone show similar spacing (cumulative frequency of approximately 50%) between 12 and 33 cm. Bioclastic grainstone has a similar distribution of spacings to ooidal/peloidal grainstone, where 25% of measurements are between 7 and 14 cm. Spicule wackestone has a higher frequency of spacings where 64% of measurements are between 0 and 14 cm, creating a tighter frequency distribution curve. Coralline limestone measurements are similar to bioclastic grainstone where 50% of measurements are between 11 and 51 cm. Rudist floatstone spacings are similar to spicule wackestone however have 17% more measurements between 0 and 9 cm, and with 5% of measurements between 25 and 41 cm.

Table 1. Summary table of stylolite network morphology statistics in sampled lithofacies.

Lithofacies Type (LFT)	Characteristic Components	Sedimentary Features	Stylolite Spacing (cm)	Stylolite Amplitude (cm)	Stylolite Wavelength (cm)	Intersection Density (X- & Y-type p/m)	Anastomosis Angle (°)
Dolostone	Miliolids	Idiotopic texture, metre-scale bedding	18.6	1.6	10.7	5	n/a
Bioclastic Grainstone	Peloids, foraminifera miliolids, orbitolinids, bivalve fragments	Good sorting, decimetre-scale bedding	13.9	1.2	11.1	7	n/a
Ooidal / Peloidal Grainstone	Ooids, peloids, miliolids, echinoderms	Good sorting, centimetre-scale bedding	17.0	1.2	11.6	6	n/a
Coral Limestone	Corals, peloids, bivalves	Poor sorting, metre-scale bedding	132.0	2.0	12.0	11	46
Bioclastic Wacke / Packstone	foraminifera orbitolinids, miliolids, bivalves, peloids, echinoderms	Poor sorting, decimetre-scale bedding	6.1	1.6	10.9	8	42
Rudist Floatstone	Rudists, other bivalves, echinoderms	Poor sorting, metre-scale bedding	10.9	1.6	8.5	6	80
Spicule Wackestone	Spicules, bivalves, foraminifera	Moderate sorting, metre-scale bedding	12.6	1.5	11.5	4	92

Bioclastic wackestone/packstone and spicule wackestone have similar amplitude measurements, where approximately 25% of measurements are between 0 and 1 cm and 65% are between 1 and 2.4 cm. Rudist floatstone has 15% of measurements between 2.2 and 4.4 cm, similar to spicule wackestone, however has fewer measurements (40% compared to 50% respectively) between 0 and 1.4 cm. Dolostone has a similar amplitude distribution to mud-

supported lithofacies, particularly bioclastic wackestone/packstone, where 50% of measurements are between 1.2 and 2.6 cm. Grain-supported lithofacies, bioclastic grainstone and ooidal/peloidal grainstone, have approximately 50% of amplitude measurements between 0 and 1.2 cm which is 12-30% higher than all other sampled lithofacies. Coralline limestone has 50% of amplitude measurements between 0 and 1.8 cm which is the lowest of all sampled lithofacies, however 10% of measurements are between 3.6 and 8.2 cm which is higher than all sampled lithofacies.

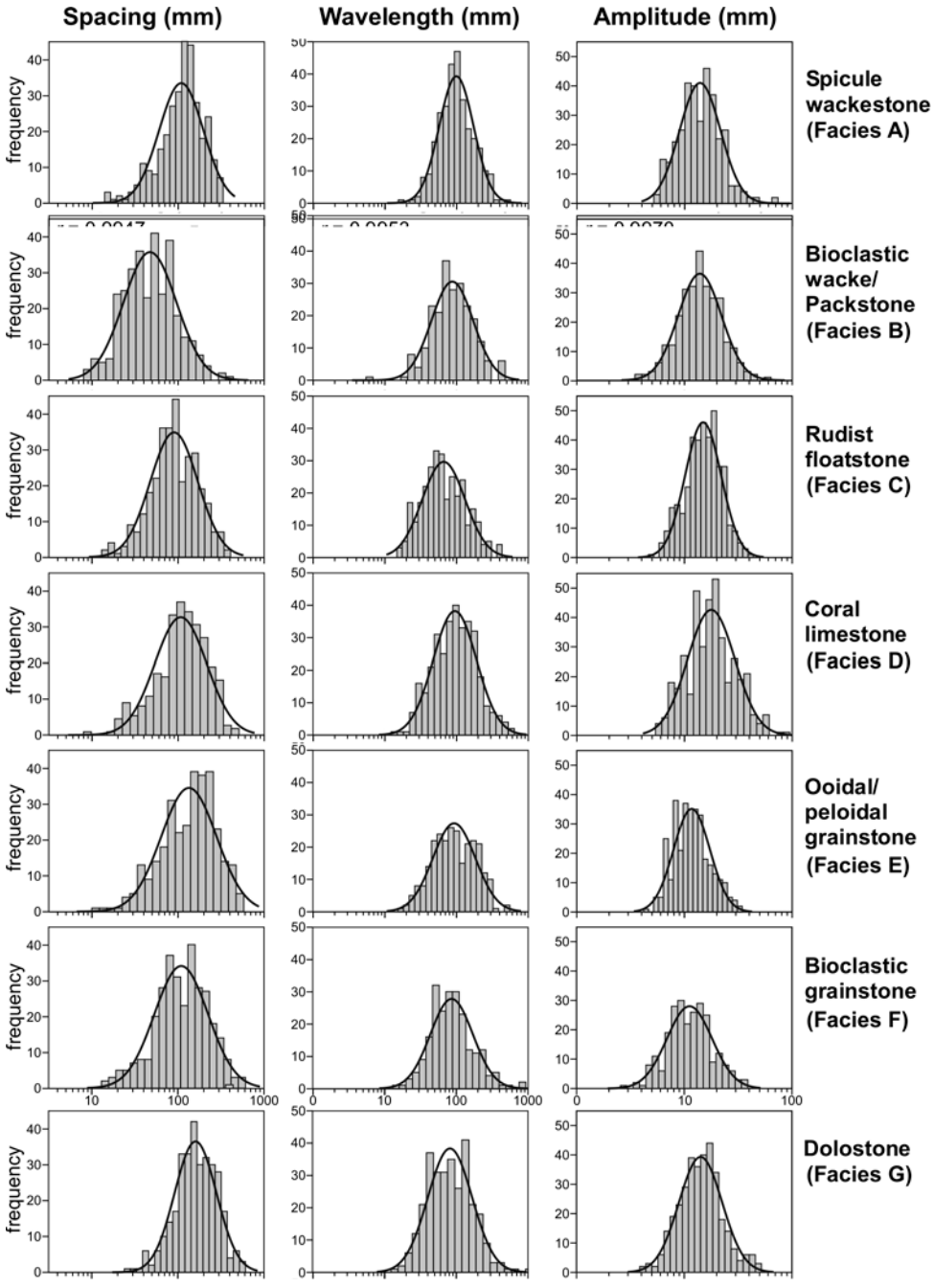

Fig. 9. Histograms of log-normal stylolite spacing, amplitude and wavelength measurements per sampled lithofacies.

Stylolite populations across all lithofacies share similarities in the distribution of wavelength measurements, where approximately 50% of all wavelength measurements across

all lithofacies range between 1.3 and 10 cm (Fig. 9). Rudist floatstone shows the largest variation in wavelength compared to other lithofacies, with 50% of measurements varying between 1.5 and 6 cm. Dolostone, ooidal/peloidal grainstone and bioclastic grainstone share similar wavelength distributions compared to other lithofacies.

Based on the classification scheme by Koehn et al. (2016) stylolites predominantly have a suture and sharp-peak type morphology throughout all sampled lithofacies (Fig. 10). Stylolites with a suture and sharp-peak type morphology account for over 80% of sampled stylolites per lithofacies, apart from bioclastic grainstone, whilst wave-like type stylolites account for 2 – 48 % per lithofacies. Wave-like type stylolites are most abundant in spicule wackestone and ooidal/peloidal grainstones compared to other lithofacies (15 % and 48 % respectively). Rectangular layer type stylolites are the least abundant type of stylolite morphology with relative abundances of 3 % - 16 %, with the highest recorded abundance in ooidal/peloidal grainstone.

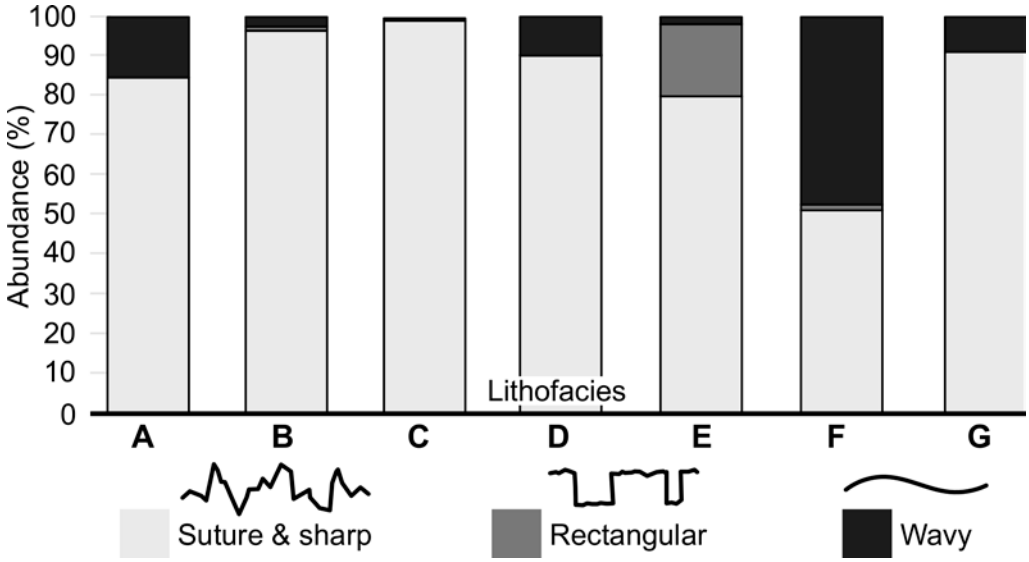

Fig. 10. Percentage abundances of stylolite morphology using the classification scheme by Koehn *et al*. (2016).

Stylolite distribution fitting shows that spacing, amplitude and wavelength measurements are all best represented by a log-normal distribution (Figs. 9, 11), rejecting the null hypothesis with *p*-values greater than 0.05. For spacing measurements (Figs. 9,11a), a log-normal distribution produced chi-squared values between 3.60 and 7.56, whereas power-law and exponential distributions have higher values of >220, signifying a reduced goodness of fit. KS-test results with a *p*-value greater than 0.05 indicates a higher goodness of fit between the fitted distribution and stylolite dataset. Log-normal distribution *p*-values are all greater than 0.05, whilst power-law and exponential are 0, indicating that spacing measurements are significantly different compared to these distributions. Rudist floatstone and ooidal/peloidal grainstones have the lowest *p*-values (0.36 and 0.26) for a log-normal distribution, whilst all other lithofacies have values of >0.75, indicating a stronger fit. Stylolite amplitude measurements have a similar range of chi-squared values (Fig. 9, 11b), from 3.47 to 11.85, with grain-supported lithofacies sharing similar values between 5.2 and 6.2. Chi-squared values from exponential and power-law distributions are >492, indicating a poor fit. Most lithofacies have log-normal distributions with high *p*-values of >0.66. However, rudist floatstone has a value of 0.36. No clear trend is evident between log-normal

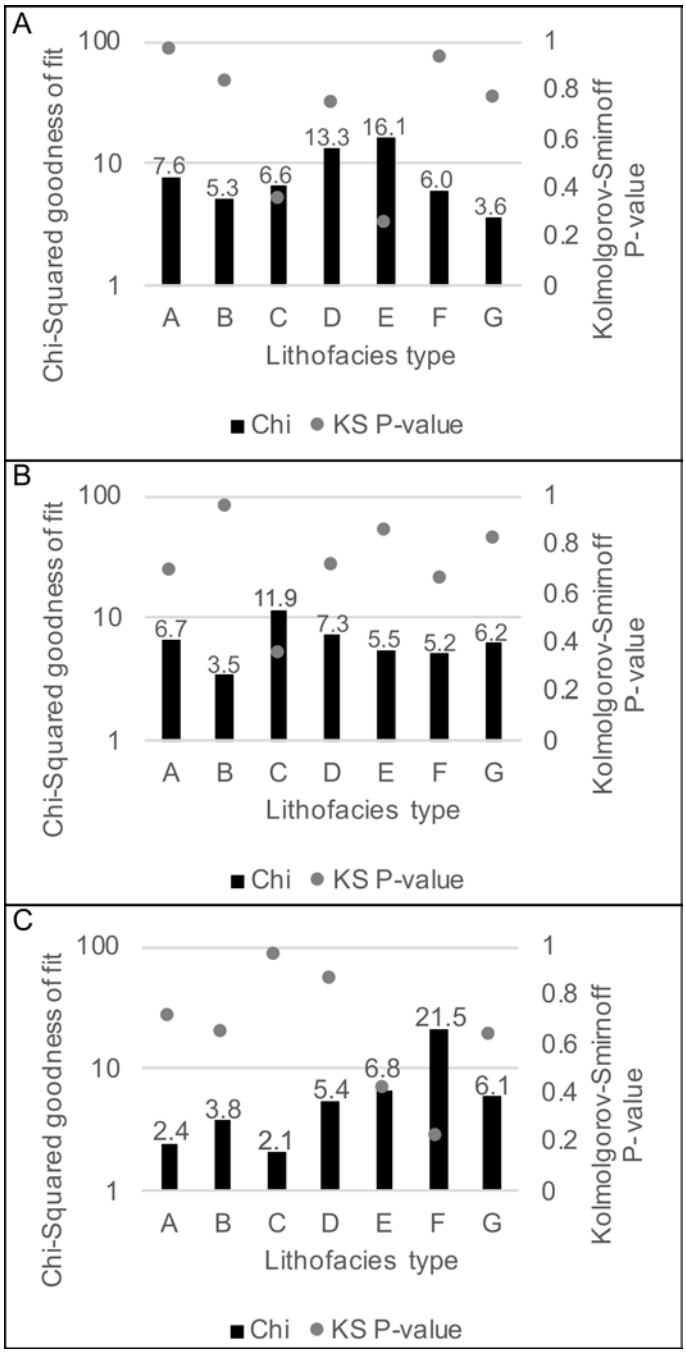

Fig. 11. Log-normal distribution fitting results for stylolite measurements using chi-squared and Kolmogorov-Smirnoff (K-S) normality test. (A) Spacing measurements. (B) Amplitude measurements. (C) Wavelength measurements.

p-values and the rock composition. Stylolite wavelength measurements have chi-squared values that are typically low (Fig. 11c), between 2.13 and 6.83, but bioclastic grainstone has a relatively large value of 21.50. Chi-squared values are all lower in mud-supported lithofacies in comparison to grain-supported lithofacies. Power-law and exponential distributions have chi-squared values of >98, indicating a poor fit. KS-test results have a distribution of *p*-values between 0.23 and 0.97, where mud-supported lithofacies have higher values relative to grain-supported lithofacies. Power-law and exponential distribution *p*-values are all zero, but values for an exponential distribution in rudist floatstone are 0.052, indicating that rudist floatstone

wavelength data are not significantly different from those of an exponential distribution. The *p*-value of a log-normal distribution for rudist floatstone is still significantly higher (0.97). However, an exponential distribution can also be weakly representative.

For lithofacies intersections (Fig. 5, 12a) spicule wackestone features the highest proportion of X-type intersections (16%) with other lithofacies having between 5 and 12% X-type intersections. X-type intersection abundances tend to not fluctuate. Coralline limestone is the anomaly in this trend. Lithofacies have an intersection density per metre of 0.7 to 5.2. Intersection density is higher in mud-supported facies (Fig. 12b). Variations in density occur between grain- and mud-supported lithofacies. Mud-supported facies have an intersection density of 2.6 to 5.2 per metre whereas grain-supported facies have 0.7 to 1.2 per metre.

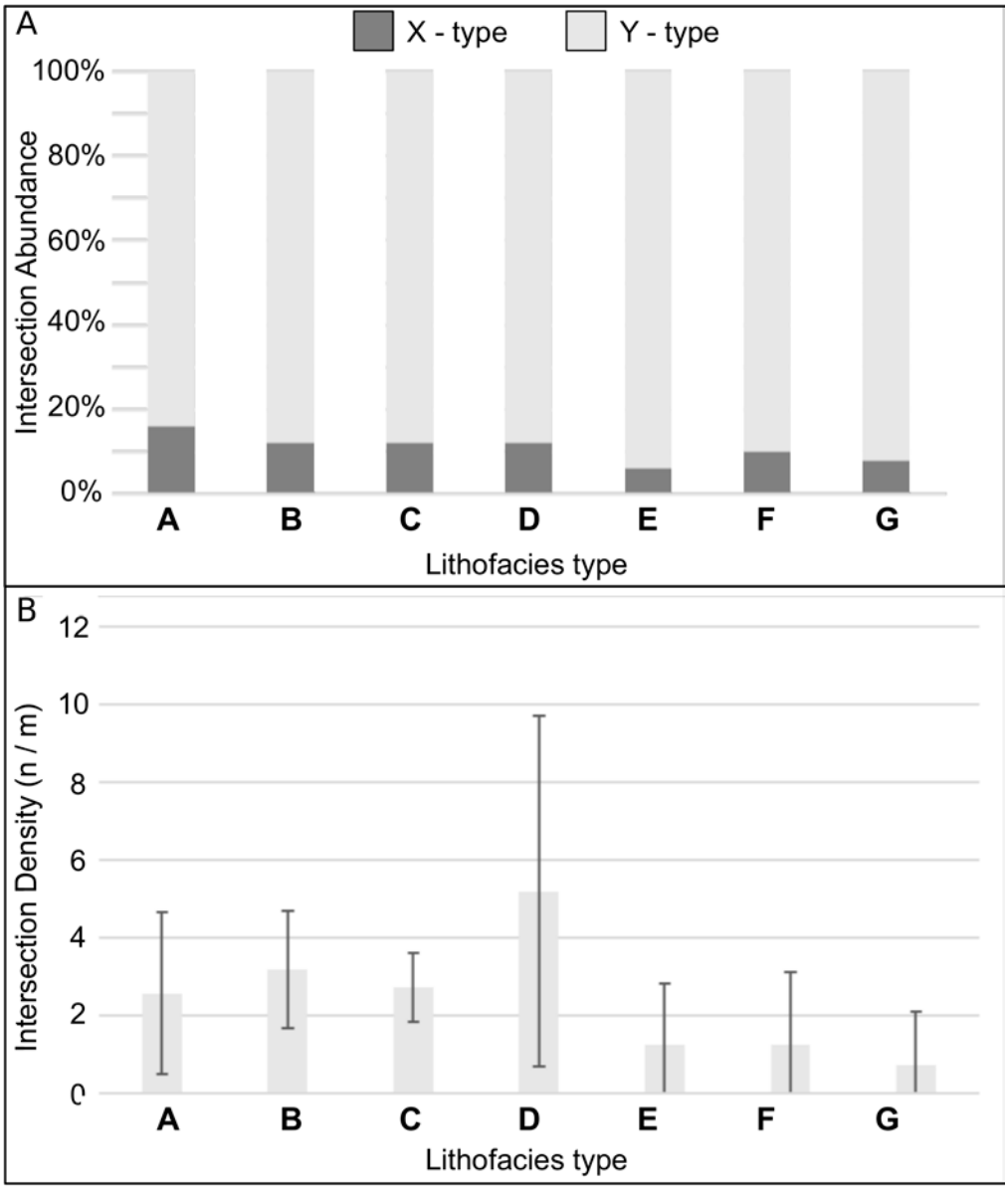

Fig. 12. (A) Stacked chart of stylolite intersection abundance in studied lithofacies. (B) Stylolite intersection density plot for each lithofacies.

4.4. Stylolite connectivity

Stylolite island dimensions in the studied lithofacies range in length and width between 1-71 cm and 1-17 cm, respectively (Fig. 13). Coralline limestone and bioclastic wackestone/packstone have the smallest range of length and width measurements (50 cm and 14 cm) (Fig. 13a, b) and therefore the smallest stylolite islands. Comparatively, rudist floatstone and spicule wackestone measurements are larger and with an increased spread of measurements when stylolite lengths are above 20 cm (Fig. 13c, d). When comparing the length to width ratio of stylolite islands it is apparent that coralline limestone has the largest range of 14.4 whilst rudist floatstone has the lowest at 7.

Spicule wackestone has the largest island areas with a mean average of 50 cm^2 (Fig. 13d), compared to other lithofacies in which this value ranges between 8.1 cm^2 and 13.9 cm^2. Coralline limestone and bioclastic wackestone/packstone and have similar mean average areas (9.2 cm^2 and 8.1 cm^2), indicating minimal variation in island area (Fig. 13a, b). Rudist floatstone and coralline limestone have similar ranges and standard deviations (Table 2), whereas spicule wackestone has both the largest range and standard deviation indicating a wide distribution of island area measurements.

Coralline limestone intersection angles show the strongest decrease with distance, with an average angle of 46° (Fig. 14a). Bioclastic wackestone/packstone shares this trend by showing a decrease in intersection angle with distance. However, intersection angles do not begin as high as in coralline limestone resulting in an intersection angle of 42° (Fig. 14b). Alternatively, both rudist floatstone and spicule wackestone stylolite networks have much steeper intersection angles which weakly decrease with distance from stylolite intersection (Fig. 14 c, d).

Table 2. Summary of stylolite island area statistics for four sampled lithofacies.

	Mean (cm)	Range (cm)	Standard Deviation (cm)
Spicule wackestone	49.8	216.7	53.9
Bioclastic wackestone / packstone	9.2	38.9	9.7
Rudist floatstone	13.9	98.8	17.0
Coralline limestone	8.1	144.4	16.6

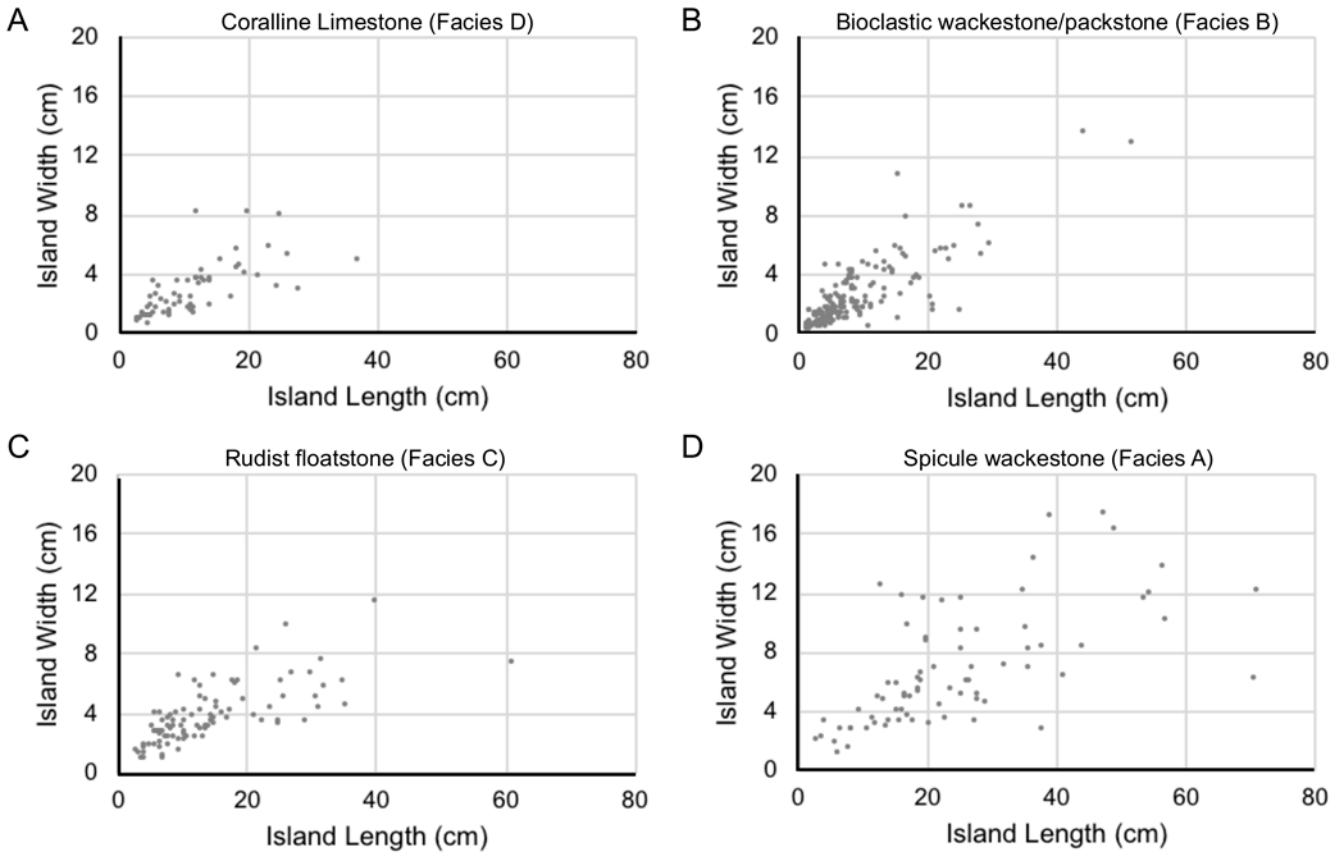

Fig. 13. Stylolite island dimension plots per sampled lithofacies. (A) Coralline limestone. (B) Bioclastic wackestone/packstone. (C) Rudist floatstone. (D) Spicule wackestone.

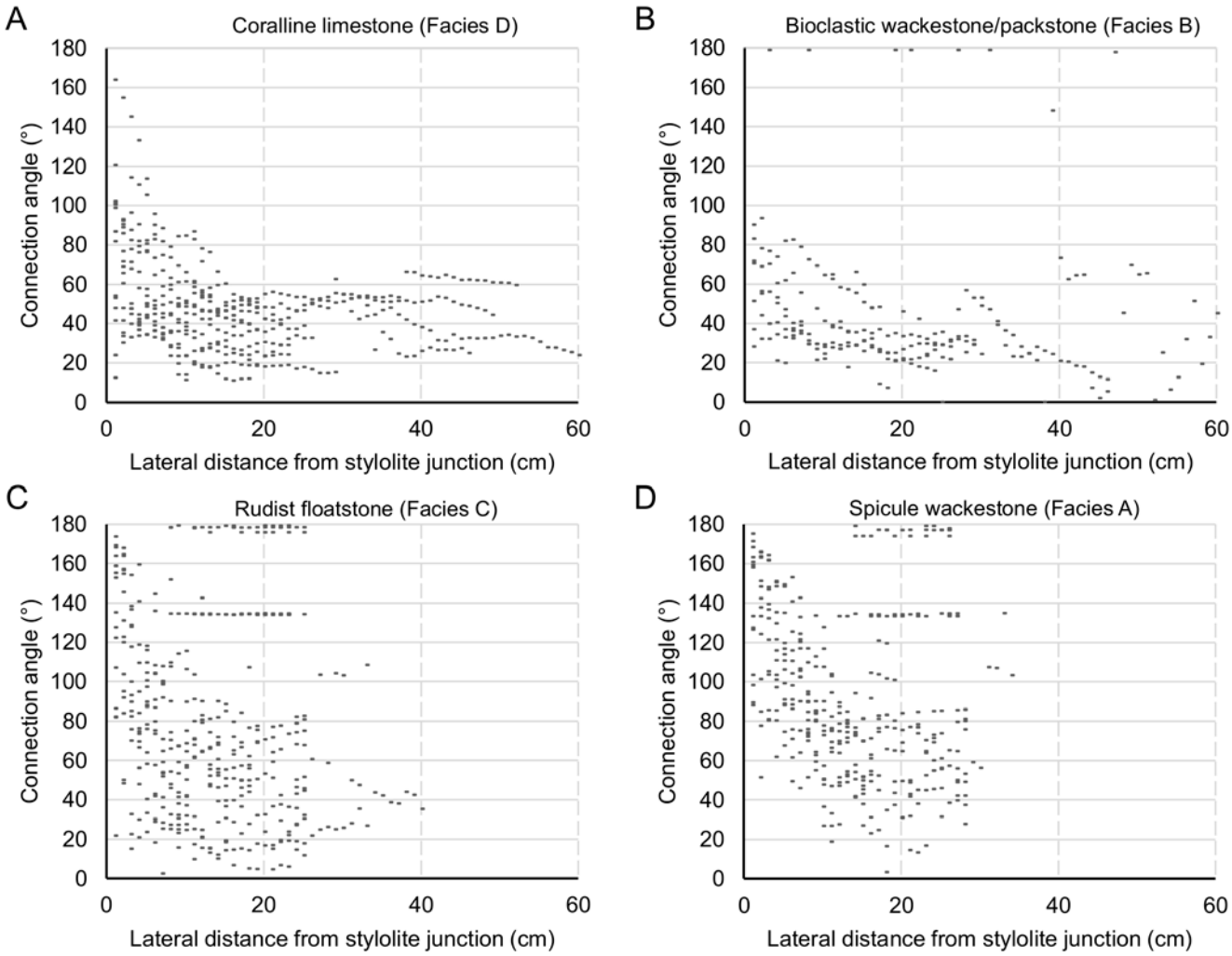

Fig. 14. Stylolite intersection angle plots per sampled lithofacies. (A) Coralline limestone. (B) Bioclastic wackestone/packstone. (C) Rudist floatstone. (D) Spicule wackestone.

5. Discussion

5.1. Correlation Analysis

In order to characterise stylolite populations as a function of lithofacies through statistical correlation analysis, it is important to firstly characterise the lithofacies parameters that enable comparison between specific lithological and morphological features. Observations from petrographic analyses and previous work by Martín-Martín et al. (2013) assist in both the identification of different lithological parameters and their values, allowing each lithofacies to be petrographically characterised. These parameters can be combined with stylolite morphology parameters to create a correlation matrix (Fig. 15), identifying potential relationships and influences of lithology on stylolite network geometries. The rock's degree of heterogeneity, in terms of component size, composition, sorting and bedding thickness, show distinct correlations with key stylolite morphological parameters. Poorly sorted, mud-supported lithofacies with metre-scale bedding thicknesses and heterogenous grain sizes produces high amplitude stylolite networks with low vertical spacing and wavelengths,

whereas well-sorted grain-supported lithofacies with centimetre- to decimetre-scale bedding thicknesses produce stylolites with low amplitudes and larger vertical spacings.

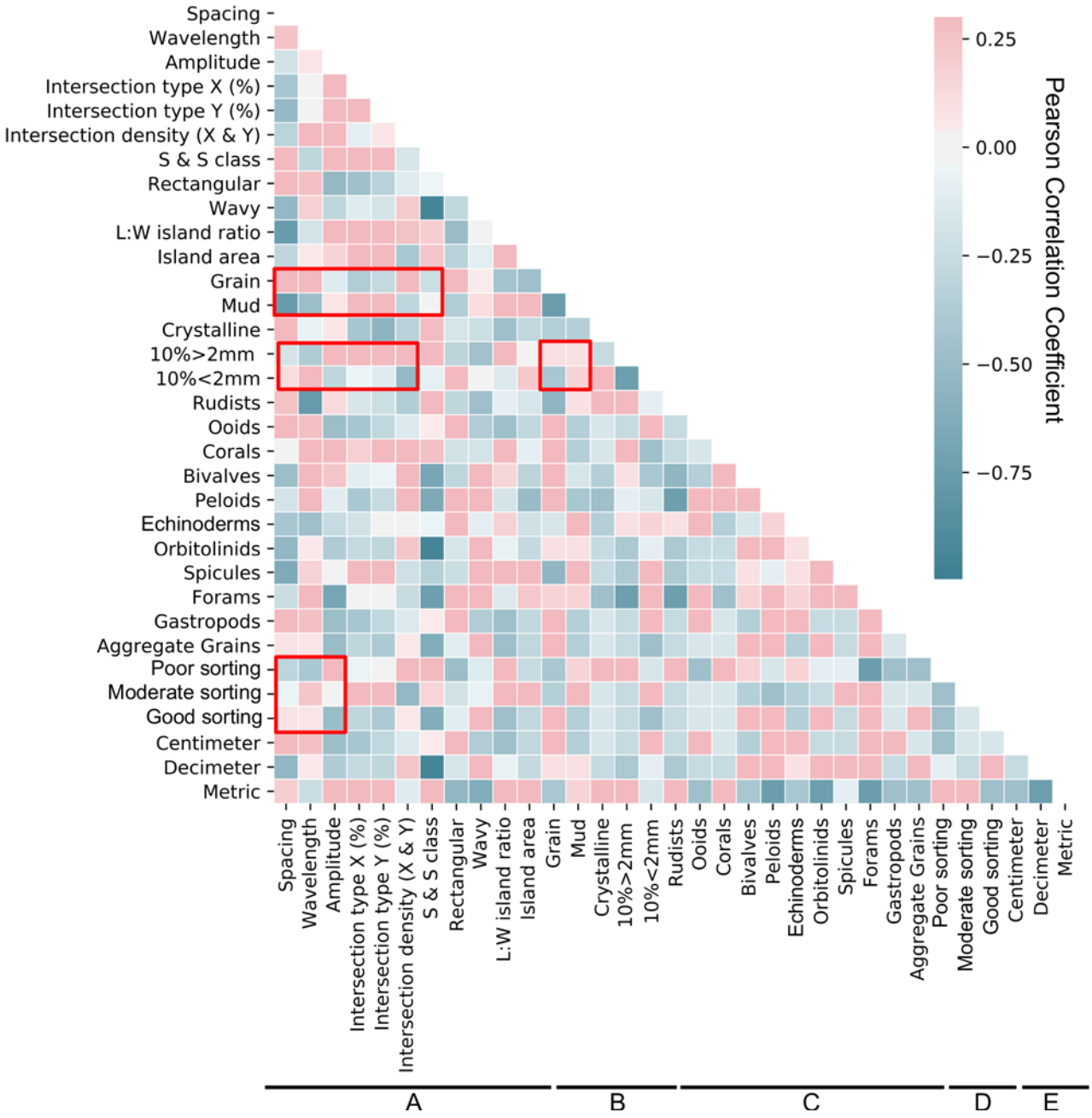

Fig. 15. Correlation matrix evaluating measuring the Pearson correlation coefficient between studied stylolite morphology and geological variables. Variables are classified as stylolite morphology (A), matrix (B), allochems (C), grain sorting (D) and bedding thickness scale (E). Key correlations have been highlighted (red boxes).

5.2. Statistical Analysis of Stylolite Networks

Stylolite spacing, amplitude and wavelength measurements are best represented by a log-normal distribution (Figs. 9, 11). The data are far away from a power-law distribution and the frequencies do not show power-law sections. Vandeginste and John (2013) use an

exponential distribution to represent stylolite spacing measurements, suggesting that stylolites randomly nucleate in the host rock. Despite this, our data supports work by Merino (1992) that stylolites are self-organising and influenced by spatial variations in porosity and stress. These variations primarily relate to the overall heterogeneity in the host rock, in particular the sorting of heterogenous grain compositions, which control the location of pressure solution and subsequent stylolite distribution. All sampled lithofacies are best represented by the same log-normal spacing distribution, suggesting that each lithofacies contained sufficient spatial heterogeneity to influence the sites of stylolite nucleation. Ooidal/peloidal grainstone (Facies E) has the weakest chi-squared and K-S test results for spacing (Fig. 11a), which potentially correlates with the high level of sorting in the rock resulting in less heterogeneity. However, it is worth noting that log-normal distributions of stylolite spacing could also be related to truncation bias, a type of sampling bias determined by the resolution of the sampling method (Zeeb et al., 2013). If a very thin stylolite is not identified due to outcrop conditions or because it is below the resolution of photographs then two small spacing values are removed and one larger spacing is added. This will lead to an underrepresentation of small spacings while large spacings will be overrepresented, potentially changing the spacing distribution from exponential to log-normal.

Koehn et al. (2007) and Ebner et al. (2009) associate log-normal amplitude measurements with a non-linear growth facilitated by solubility variations and subsequent grain 'pinning' (*i.e.*, where a stylolite plane is fixed to a grain or fossil). Bioclastic wackestone/packstone (Facies B) has the strongest chi-squared and K-S test results for amplitude (Fig. 9, 11b), associated with a mud-supported rock and a diverse range of grains with different compositions. When comparing distribution-fitting results with key lithological components of each lithofacies, it is apparent that there is only a weak correlation between grain size heterogeneity and the degree of sorting on stylolite amplitude. Grain-supported lithofacies generally show a reduced fit compared to mud-supported lithofacies when examining both chi-squared and KS results for log-normal stylolite distributions. These grain-supported lithofacies, including ooidal/peloidal grainstone (Facies E), bioclastic grainstone (Facies F) and dolostone (Facies G) (which is interpreted to have had a grain-supported precursor texture before dolomitisation), are all well sorted with lower compositional heterogeneity. The lack of heterogeneity may therefore re-emphasise the importance of solubility variations on stylolite amplitude as previously suggested by Ebner et al. (2009), where the absence of sufficient grain 'pinning' reduces non-linear amplitude growth. Stylolite wavelength measurements have stronger chi-squared and K-S test results in lithofacies with a mud-supported rock (Fig. 9, 11c) which could be related to clay content, providing enhanced dissolution as proposed by Aharonov and Katsman (2009), and therefore spatial solubility variations which also influence amplitude growth.

5.3. Lithological Influences on Stylolite Morphology

Key relationships influencing stylolite morphology can be derived from the correlation matrix of host rock lithological parameters (Fig. 15). Where previous work has focused on identifying the influences of different types of rock heterogeneity on the degree of stylolite suturing, this study can effectively evaluate specific heterogeneities and their influences on a variety of stylolite morphological parameters.

5.3.1. Mud- versus grain-dominated facies

The presence of micrite and clay minerals has often been identified as a major cause of heterogeneity and subsequent stylolite roughening (Wanless, 1979; Koehn *et al.,* 2012; Paganoni *et al.*, 2016; Morad *et al.,* 2018). The high surface area of micrite enhances the rock's solubility. This study shows weak correlations where stylolite amplitudes (*i.e.*, roughening) vary based depending on the presence and volume of micrite and produce higher amplitudes in mud-supported facies, as recently reported by Morad *et al.* (2018). Higher amplitude stylolites facilitate more anastomosis shown by positive correlations with X- and Y-type intersections, along with smaller vertical spacing and wavelengths. Interestingly, the correlation matrix shows the opposite morphological trends when stylolites develop in grain-supported facies (Fig. 15). Clay minerals promote heterogeneity and an increase in stylolite amplitude, which is likely to cause stylolites to nucleate and intersect. This is further facilitated by the feedback loop of clay minerals and pressure-solution, as proposed by Aharonov and Katsman (2009), where the accumulation of clay minerals enhances dissolution to form stylolites which subsequently accumulate more clays.

5.3.2. Grain size, type, bedding and sorting

Other lithological parameters, aside from the presence of micrite and clay minerals, have been found to promote multifaceted heterogeneity in carbonate host rocks to subsequently impact stylolite morphology. Compositionally, bimodal grain sizes lead to increased suturing due to variations in solubility and susceptibility to pressure-solution (Railsback, 1993; Andrews and Railsback, 1997; Koehn *et al.,* 2012). Whilst stylolites are prone to develop in fine-grained carbonates (Rustichelli *et al.,* 2012), this study supports pre-existing work where lithologies with 10% of grains larger than 2 mm correlate positively with higher amplitudes (Figure 15). Additionally, there is an inverse relationship when grains are smaller than 2 mm and consequently more uniform in grain size.

Grain size variation within the stylolitised rock must also be related to the degree of sorting, where a combination of grain size variation and poor sorting will enhance the rock's heterogeneity and consequent roughness (Koehn *et al*., 2012). Poorly-sorted lithofacies are positively correlated with higher amplitude stylolites, which are more inclined to have smaller vertical spacings, abundant intersections and a higher degree of anastomosis (Fig. 15). These conditions are facilitated by variations in solubility created by grain size and distribution, causing grain pinning and differences in dissolution rates, which establish sites for stylolites to develop and roughen (Aharonov and Katsman, 2009; Koehn *et al*., 2016). Increased roughening and dissolution caused by poor sorting can also facilitate anastomosis by stylolite 'cannibalism', as suggested by Ben-Itzhak et al. (2014). The third factor influencing stylolite morphology within the rock is the type of grains present, as the composition of grains leads to solubility variations and the promotion of the stylolite development and suturing. Wanless (1979) identifies Mg as an impurity that causes solubility variations in the rock, where the degree of heterogeneity in grain composition can lead to either a uniform or varied distribution of solubility. Measurements of Mg content in fossils by Tucker and Wright (2009) can be used to establish which grains and lithofacies are likely to feature variations in Mg and therefore solubility. For example, foraminifera typically have an Mg content up to 25% whilst other fossils such as bivalves and sponges have limited ranges of 0-5% and 10-15% respectively. High or low Mg content in calcite can also facilitate differences in solubility and pressure solution, alongside additional factors influencing solubility such as calcite/aragonite content in bioclasts, the presence of non-soluble grains and silica, and the solubility of mud (Dewers and Ortleva, 1994).

The relative scale of bedding thickness was also considered for each lithofacies to identify potential influences on stylolite morphology. Stylolites are found to have smaller amplitudes and larger wavelengths as bedding changes from the metre to the centimetre scale (Fig. 9, 15), and no apparent correlation exists between vertical spacing or stylolite intersection type/density. Smaller stylolite amplitude measurements from lithofacies with centimetre-scale bedding differ from results by Sheppard (2002) and Koehn et al. (2012), who suggested that a smaller bedding scale would promote lithological contrasts to promote stylolite nucleation at bedding planes. Whilst this study shows that higher amplitude stylolites are found in lithofacies with metre-scale bedding, results may differ from the work by Sheppard (2002), since a lithofacies with centimetre-scale bedding may not have sufficient lithological contrasts which are necessary to promote stylolite nucleation at bedding planes. The depositional texture of studied lithofacies was generalised across sampling windows and supported by observations from Martín-Martín et al. (2013) and Yao (2019). Therefore, the influence of textural variations between beds on stylolite amplitude remains uncertain.

Rectangular layer type stylolites are abundant in grain-supported lithofacies with centimetre-scale bedding, such as ooidal/peloidal grainstones (Facies E). This supports work by Koehn *et al*. (2016), suggesting that rectangular layer type stylolites propagate and pin at layer interfaces. Wanless (1979) identifies grain size as the main factor that determines whether stylolites have a jagged or undulose waveform (similar to the suture and sharp-peak and wave-like types of the stylolite classification scheme), arguing that undulose waveforms tend to develop in coarse-grained lithologies. Our study observes an inverse correlation between the abundance of suture and sharp-peak and wave-like type stylolites in coarser facies (*i.e.*, 10% > 2 mm), where wave-like type stylolites develop in finer facies. A predominantly inverse correlation is also seen when evaluating the abundance of stylolite classes in relation to different allochems, where suture and sharp-peak type stylolites are more inclined to develop in facies with larger fossil grains, which again is different from observations by Koehn *et al*. (2016).

5.3.3. Stylolite Connectivity and Nucleation

The stylolites island aspect ratios quantified here show similar results to Ben-Itzhak *et al*. (2014), where islands are predominantly lenticular in shape and influenced by laterally decreasing connection angles at stylolite junctions. Spicule wackestone (Facies A) and rudist floatstone (Facies C) have higher connection angles at stylolite junctions, which Ben-Itzhak *et al*. (2014) suggest is caused by cannibalised bedding-parallel stylolite networks. Cannibalisation would be promoted by stylolite amplitude growth, in order to facilitate stylolite connectivity, and as a consequence would be expected to be more prominent in lithofacies with a large grain size heterogeneity and poor sorting. Bioclastic wackestone/packstone (Facies B) and coral limestone (Facies D) have lower connection angles, with angles more indicative of anastomosis by linking isolated discontinuous stylolites during increased dissolution (Ben-Itzhak *et al.*, 2014). A combination of clay content and grain size heterogeneity in these lithofacies would facilitate dissolution, as proposed by Aharonov and Katsman (2009) and Koehn et al. (2012). Bioclastic wackestone/packstone (Facies B) would possess both of these qualities whereas coral limestone (Facies D) would be primarily attributed to coral fragments facilitating grain size heterogeneity.

Stylolite cannibalisation requires the connection of long-parallel stylolites, which can be achieved as stylolites progressively increase in amplitude while growing. However, field

observations have shown that stylolite geometry can be altered by the presence of large fossils (Fig. 16). The contact between fossils and the matrix creates grain composition heterogeneity resulting in the formation of nucleation surfaces, in a similar way to stylolites found along bedding surfaces, to cause localised variations in stylolite geometry. A higher proportion of large fossils may facilitate the propagation of long-parallel stylolites in a perpendicular orientation, and subsequently providing a mechanism of stylolite linkage aside from amplitude growth.

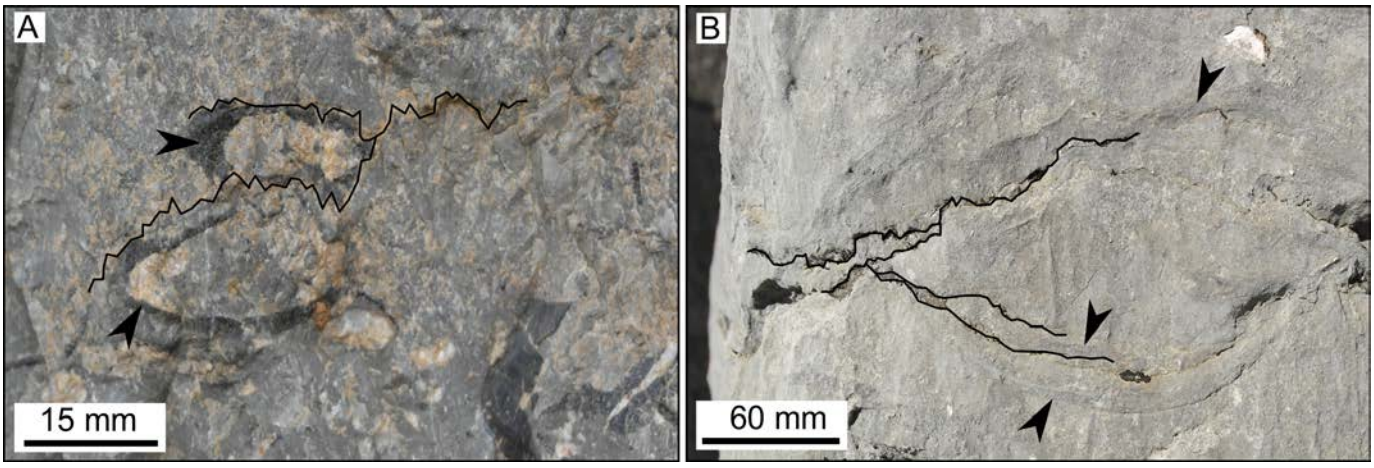

Fig. 16. Annotated field images of stylolite interactions with allochems in studied lithofacies. (A) Stylolite anastomosis between cm-scale rudists (black arrows) in a rudist floatstone. (B) stylolite nucleating along contact between *Chondrodonta* bivalves (black arrows) and matrix in a bioclastic wackestone/packstone.

Higher angle connectivity in stylolite networks results in the development of more X and Y-type intersections. Results from the correlation matrix (Fig. 15) indicates X and Y-type intersections are promoted by mud-supported facies with 10% grains larger than 2 mm and poor-to-moderate sorting. The role of larger fossils in altering stylolite geometries, as previously discussed, could additionally promote the formation of more X and Y-type intersections. However, spicule wackestone (Facies A) features similar intersection density measurements to rudist floatstone (Facies C), despite having no evident large fossils. This suggests that the presence of larger fossils cannot be primarily responsible for influencing intersection type/density and instead requires the interplay between multiple drivers of heterogeneity across multiple scales, as proposed by Koehn et al. (2016).

5.3.4. Influence of diagenesis

Aside from Mg content variations in fossil grains, the influence of diagenetic processes may alter grain composition to subsequently modify heterogeneities initially created by depositional processes. Micritisation, two early calcite cementation phases, dissolution and early stages of fracturing occurred prior to stylolitisation in the Benassal Fm (Martín-Martín *et al.*, 2015, 2017). According to these authors, stylolitisation occurred at relatively shallow burial depths and mostly predated dolomitisation of the Benassal Fm in the study area. Therefore, stylolite morphology cannot be attributed to dolostone lithofacies and is predominantly a result of the depositional texture before chemical compaction that Martín-Martín et al. (2017) interprets as being mostly grainy with minimal calcite cementation. Statistical trends from this study support this interpretation, as stylolites sampled from dolostone lithofacies share similar statistical properties with grain-supported lithofacies.

Fracturing and calcite cementation were observed from petrographic analysis, although their interaction with stylolite formation could not be fully characterised as 1) the absence of clear cross-cutting relationships between stylolites and fractures makes it difficult to ascertain relative timing and therefore influences on stylolite morphology, and 2) calcite cementation in this study was not characterised using the paragenetic sequence nomenclature of Martín-Martín et al. (2017) which again makes it difficult to estimate relative timings and influences on stylolites. Fracturing initiated during the onset of Early Cretaceous rifting (Gomez-Rivas *et al*., 2012; Martín-Martín *et al*., 2015) and therefore did not coincide with stylolitisation that Martín-Martín et al., (2015) estimate started in the Late Cretaceous.

6. Conclusions

Stylolite networks were statistically characterised according to morphological variations in various typical shallow-marine carbonate platform lithofacies. The spacing, wavelength and amplitude of stylolites follow a log-normal distribution for all the studied lithofacies. Multiple sources of lithological heterogeneity were identified and related to stylolite morphology. Specifically, the interplay between grain sizes above 2 mm, heterogenous grain compositions, poor sorting and metre-scale bed thicknesses resulted in the formation of high-amplitude stylolites which are closely spaced and feature a high level of anastomosis (Fig. 17a). These stylolite networks are typically found in bioclastic wackestone/packstone, rudist floatstone and spicule wackestone, whereas isolated stylolites with larger spacings and low amplitudes are found in lithofacies with limited heterogeneity, such as bioclastic grainstone, ooidal/peloidal grainstone and dolostone (Fig. 17b). Stylolite networks produced in lithofacies that contain large grains (*e.g.*, coralline limestone) have moderate amplitudes and wavelength with wavelengths, and have closer spacings than other grain-dominated lithofacies (Fig. 17c). The extent of stylolite network connectivity, and their subsequent potential control on fluid flow, can therefore be primarily determined by the characteristics of the host lithofacies.

A

Lithofacies	Matrix type	Grain size	Grain Composition	Grain Sorting	Bedding Scale
Spicule Wackestone (A)	Mud	10 % < 2 mm	High	Poor	Meter
Bioclastic Wackestone / Packstone (B)	Mud	10 % < 2 mm	High	Poor	Meter
Rudist Floastone (C)	Mud	10 % < 2 mm	Moderate	Poor	Meter
Coralline Limestone (D)	Grain	10 % > 2 mm	Moderate	Moderate	Meter
Ooidal / Peloidal Grainstone (F)	Grain	10 % > 2 mm	Moderate	Well	Decimeter
Bioclastic Grainstone (E)	Grain	10 % > 2 mm	Moderate	Well	Decimeter
Dolostone (F)	Crystalline	10 % < 2 mm	Low	Well	Centimeter

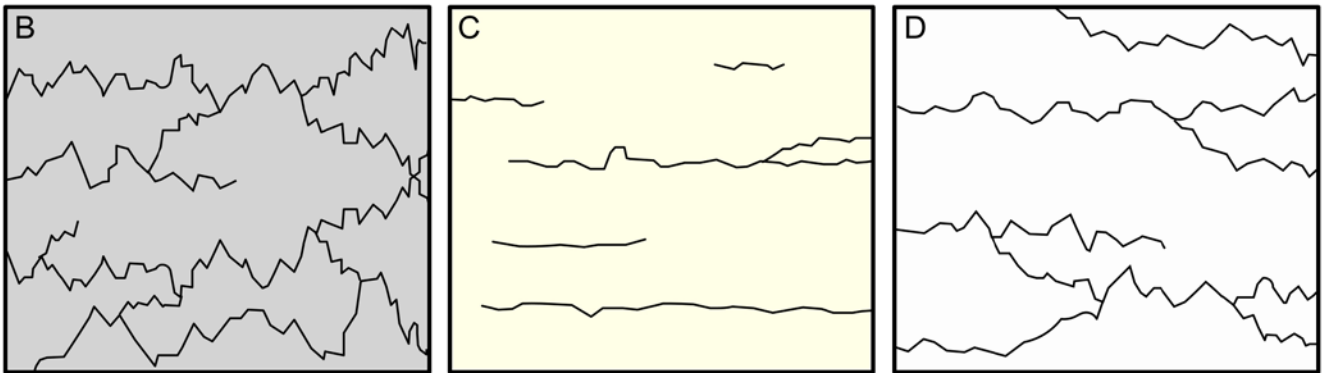

Fig. 17. Diagram of typical stylolite network morphologies observed in studied lithofacies. (A) Example of stylolite networks produced in mud-dominated facies (spicule wackestone, bioclastic wackestone, rudist floatstone) where stylolites are high amplitude, high wavelength, closely spaced and highly anastomosing with frequent X- and Y-type intersections. (B) Example of stylolite networks produced in grain-dominated facies (ooidal/peloidal grainstone, bioclastic grainstone and including dolostone) where stylolites are low amplitude and wavelength with large vertical spacings. Stylolites develop isolated long-parallel networks. (C) Example of stylolite networks produced in lithofacies with large grain components (coralline limestone) where stylolite networks have moderate amplitudes and wavelength with closer spacings than other grain-dominated lithofacies. Minor amounts of X- and Y-type intersections which creates long-parallel to slightly anastomosing networks with a branching appearance.

Acknowledgements

This research was funded by the Natural Environment Research Council (NERC) Centre for Doctoral Training (CDT) in Oil & Gas, through a PhD grant to EH. Additional funding was provided by the Grup Consolidat de Recerca "Geologia Sedimentària" (2017SGR-824) and the DGICYT Spanish Projects CGL2015-66335-C2-1-R, CGL2015-69805-P and PGC2018-093903-B-C22. EGR acknowledges the support of the Beatriu de Pinós programme of the Government of Catalonia's Secretariat for Universities and Research of the Department of Economy and Knowledge (2016 BP 00208). We are grateful to anonymous reviewers, whose constructive comments have improved the article, together with the editorial guidance of Miroslaw Slowakiewicz.

References

Aharonov, E. and Katsman, R., 2009. Interaction between pressure solution and clays in stylolite development: Insights from modeling. *American Journal of Science*, *309*(7), 607-632.

Agar, S.M. and Geiger, S., 2015. Fundamental controls on fluid flow in carbonates: current workflows to emerging technologies. *Geological Society, London, Special Publications*, *406*(1), 1-59.

Alsharhan, A.S., Sadd, J., 2000. Stylolites in lower Cretaceous carbonate reservoirs, U.A.E.. *Soc. Econ. Paleontol. Mineral. Special* Publication 69, 185–207.

Andrews, L.M. and Railsback, L.B., 1997. Controls on stylolite development: morphologic, lithologic, and temporal evidence from bedding-parallel and transverse stylolites from the US Appalachians. *The Journal of Geology*, *105*(1), 59-73.

Barnett, A.J., Wright, V.P., Chandra, V.S., Jain, V., 2015. Distinguishing between eogenetic, unconformity-related and mesogenetic dissolution: a case study from the Panna and Mukta fields, offshore Mumbai, India. *Geological Society, London, Special Publications*, 435(1): 67.

Baron, M. and Parnell, J., 2007. Relationships between stylolites and cementation in sandstone reservoirs: Examples from the North Sea, UK and East Greenland. *Sedimentary Geology*, *194*(1), 17-35.

Baud, P., Rolland, A., Heap, M., Xu, T., Nicolé, M., Ferrand, T., Reuschle, T., Toussaint, R. and Conil, N., 2016. Impact of stylolites on the mechanical strength of limestone. *Tectonophysics*, *690*, 4-20.

Bäuerle, G., Bornemann, O., Mauthe, F. and Michalzik, D., 2000. Origin of stylolites in Upper Permian Zechstein anhydrite (Gorleben salt dome, Germany). *Journal of Sedimentary Research*, *70*(3). 726-737.

Ben-Itzhak, L.L., Aharonov, E., Karcz, Z., Kaduri, M. and Toussaint, R., 2014. Sedimentary stylolite networks and connectivity in limestone: Large-scale field observations and implications for structure evolution. *Journal of Structural Geology*, *63*, 106-123.

Bergen, D.V. and Carozzi, A.V., 1990. Experimentally simulated stylolitic porosity in carbonate rocks. *Journal of Petroleum Geology*, *13*(2), 179-192.

Burgess, C.J. and Peter, C.K., 1985. Formation, distribution, and prediction of stylolites as permeability barriers in the Thamama Group, Abu Dhabi. *Middle East Oil Technical Conference and Exhibition*. Society of Petroleum Engineers (SPE-13698-MS).

Bruna, P.O., Lavenu, A.P., Matonti, C. and Bertotti, G., 2019. Are stylolites fluid-flow efficient features?. *Journal of Structural Geology*, *125*, 270-277.

Carozzi, A.V. and Bergen, D.V., 1987. Stylolitic porosity in carbonates: a critical factor for deep hydrocarbon production. *Journal of Petroleum Geology*, *10*(3), 267-282.

Corbella, M., Gomez-Rivas, E., Martín-Martín, J.D., Stafford, S.L., Teixell, A., Griera, A., Travé, A., Cardellach, E. and Salas, R., 2014. Insights to controls on dolomitization by means of reactive transport models applied to the Benicàssim case study (Maestrat Basin, eastern Spain). *Petroleum Geoscience*, *20*(1), 41-54.

Chandra, V., Wright, P., Barnett, A., Steele, R., Milroy, P., Corbett, P., Geiger, S. and Mangione, A., 2015. Evaluating the impact of a late-burial corrosion model on reservoir permeability and performance in a mature carbonate field using near-wellbore upscaling. *Geological Society, London, Special Publications*, *406*(1), 427-445.

Dawson, W.C., 1988. Stylolite porosity in carbonate reservoirs (No. CONF-880301-). *American Association of Petroleum Geologists*, Tulsa, OK.

Dewers, T., Ortoleva, P., 1994. Formation of stylolites, marl/limestone alternations, and dissolution (clay) seams by unstable chemical compaction of argillaceous carbonates. In: Wolf, K.H., Chilingarian, G.V. (Eds.), Diagenesis: IV. *Developments in Sedimentology, 51*, 155–216.

Di-Cuia, R., Gout, C., Balzagette, L., Masse, P. and Vieban, F., 2005. Reservoir Connectivity in a Complex Fractured Reservoir: The Relationship Between Fracturing and Facies in the Upper Cretaceous Apulian Platform of the Maiella Mountain, Southern Italy. In *International Petroleum Technology Conference*. International Petroleum Technology Conference.

Ebner, M., Koehn, D., Toussaint, R., Renard, F., 2009. The influence of rock heterogeneity on the scaling properties of simulated and natural stylolites. *Journal of Structural Geology*, *31*(1), 72-82.

Ebner, M., Piazolo, S., Renard, F. and Koehn, D., 2010. Stylolite interfaces and surrounding matrix material: Nature and role of heterogeneities in roughness and microstructural development. *Journal of Structural Geology*, *32*(8), 1070-1084.

Ehrenberg, S.N., Morad, S., Yaxin, L. and Chen, R., 2016. Stylolites and Porosity, In A Lower Cretaceous Limestone Reservoir, Onshore Abu Dhabi, UAE. *Journal of Sedimentary Research*, *86*(10), 1228-1247.

Fabricius, I.L., 2014. Burial stress and elastic strain of carbonate rocks. *Geophysical Prospecting*, *62*(6), 1327-1336.

Finkel, E.A. and Wilkinson, B.H., 1990. Stylolitization as Source of Cement in Mississippian Salem Limestone, West-Central Indiana (1). *AAPG Bulletin*, *74*(2), 174-186.

Gomez-Rivas, E., Corbella, M., Martín-Martín, J.D., Stafford, S.L., Teixell, A., Bons, P.D., Griera, A. and Cardellach, E., 2014. Reactivity of dolomitizing fluids and Mg source evaluation of fault-controlled dolomitization at the Benicassim outcrop analogue (Maestrat Basin, E Spain). *Marine and Petroleum Geology*, *55*, 26-42.

Gomez-Rivas, E., Martín-Martín, J.D., Bons, P.D. and Koehn, D., 2015. Can stylolite networks control the geometry of hydrothermal alterations? *Geotectonic Res*, *97*, 34-36.

Gomez-Rivas, E., Warber, K., Kulzer, F., Bons, P.D., Koehn, D. and Martín, J.D.M., 2012. Structural evolution of the Benicàssim area (Maestrat basin, NE Spain): insights from fracture and vein analysis. *Geogaceta*, (51), 79-82.

Guerriero, V., Mazzoli, S., Iannace, A., Vitale, S., Carravetta, A. and Strauss, C., 2013. A permeability model for naturally fractured carbonate reservoirs. *Marine and Petroleum Geology*, *40*, 115-134.

Guimerà, J., Mas, R. and Alonso, Á., 2004. Intraplate deformation in the NW Iberian Chain: Mesozoic extension and Tertiary contractional inversion. *Journal of the Geological Society*, *161*(2), 291-303.

Haines, T.J., Michie, E.A., Neilson, J.E. and Healy, D., 2016. Permeability evolution across carbonate hosted normal fault zones. *Marine and Petroleum Geology*, *72*, 62-82.

Hammer, Ø., Harper, D.A.T., Ryan, P.D., 2001. PAST: Paleontological statistics software for education. folk.uio.no/ohammer/past.

Harris, N.B., 2006. Low-porosity haloes at stylolites in the feldspathic Upper Jurassic Ula sandstone, Norwegian North Sea: an integrated petrographic and chemical mass-balance approach. *Journal of Sedimentary Research*, *76*(3), 444-459.

Hassan, T.H. and Wada, Y., 1981. Geology and development of Thamama zone 4, Zakum field. *Journal of Petroleum Technology*, *33*(07), 1-327

Heap, M.J., Baud, P., Reuschlé, T. and Meredith, P.G., 2014. Stylolites in limestones: Barriers to fluid flow?. *Geology*, *42*(1), 51-54.

Heap, M., Reuschlé, T., Baud, P., Renard, F. and Iezzi, G., 2018. The permeability of stylolite-bearing limestone. *Journal of Structural Geology*, *118*, 81-93.

Humphrey, E., Rivas, E.G., Koehn, D., Bons, P.D., Neilson, J., Martin-Martin, J. and Schoenherr, J., 2019. Stylolite-controlled diagenesis of a mudstone carbonate reservoir: A case study from the Zechstein_2_Carbonate (Central European Basin, NW Germany). *Marine and Petroleum Geology*, *109*, 88-107.

Koehn, D., Ebner, M., Renard, F., Toussaint, R. and Passchier, C.W., 2012. Modelling of stylolite geometries and stress scaling. *Earth and Planetary Science Letters*, *341*, 104-113.

Koehn, D., Renard, F., Toussaint, R. and Passchier, C.W., 2007. Growth of stylolite teeth patterns depending on normal stress and finite compaction. *Earth and Planetary Science Letters*, *257*(3), 582-595.

Koehn, D., Rood, M.P., Beaudoin, N., Chung, P., Bons, P.D. and Gomez-Rivas, E., 2016. A new stylolite classification scheme to estimate compaction and local permeability variations. *Sedimentary Geology*, *346*, 60-71.

Larsen, B., Grunnaleite, I. and Gudmundsson, A., 2010. How fracture systems affect permeability development in shallow-water carbonate rocks: an example from the Gargano Peninsula, Italy. *Journal of Structural Geology*, *32*(9), 1212-1230.

Laubach, S.E., Olson, J.E. and Gross, M.R., 2009. Mechanical and fracture stratigraphy. *AAPG bulletin*, *93*(11), 1413-1426.

Liesa, C.L., Soria, A.R., Meléndez, N. and Meléndez, A., 2006. Extensional fault control on the sedimentation patterns in a continental rift basin: El Castellar Formation, Galve sub-basin, Spain. *Journal of the Geological Society*, *163*(3), 487-498.

Lind, I., Nykjaer, O., Priisholm, S. and Springer, N., 1994. Permeability of stylolite-bearing chalk. *Journal of Petroleum Technology*, *46*(11), 986-993.

Long, J. and Witherspoon, P.A., 1985. The relationship of the degree of interconnection to permeability in fracture networks. *Journal of Geophysical Research: Solid Earth*, *90*(B4), 3087-3098.

Manzocchi, T., 2002. The connectivity of two-dimensional networks of spatially correlated fractures. *Water Resources Research*, *38*(9).

Martín-Martín, J.D., Gomez-Rivas, E., Bover-Arnal, T., Travé, A., Salas, R., Moreno-Bedmar, J.A., Tomás, S., Corbella, M., Teixell, A., Vergés, J. and Stafford, S.L., 2013. The Upper Aptian to Lower Albian syn-rift carbonate succession of the southern Maestrat Basin (Spain): Facies architecture and fault-controlled stratabound dolostones. *Cretaceous Research*, *41*, 217-236.

Martín-Martín, J.D., Travé, A., Gomez-Rivas, E., Salas, R., Sizun, J.P., Vergés, J., Corbella, M., Stafford, S.L. and Alfonso, P., 2015. Fault-controlled and stratabound dolostones in the Late Aptian–earliest Albian Benassal Formation (Maestrat Basin, E Spain): petrology and geochemistry constrains. *Marine and Petroleum Geology*, *65*, 83-102.

Martín-Martín, J.D., Gomez-Rivas, E., Gómez-Gras, D., Travé, A., Ameneiro, R., Koehn, D. and Bons, P.D., 2017. Activation of stylolites as conduits for overpressured fluid flow in dolomitized platform carbonates. *Geological Society, London, Special Publications*, *459*(1), 157-176.

Massey, F.J., 1951. The Kolmogorov-Smirnov test for goodness of fit. *Journal of the American statistical Association*, *46*(253), 68-78.

Merino, E., 1992. Self-organization in stylolites. *American Scientist*, *80*(5), 466-473.

Morad, D., Nader, F.H., Morad, S., Al Darmaki, F. and Hellevang, H., 2018. Impact of Stylolitization On Fluid Flow and Diagenesis in Foreland Basins: Evidence from an Upper Jurassic Carbonate Gas Reservoir, Abu Dhabi, United Arab Emirates. *Journal of Sedimentary Research*, *88*(12), 1345-1361.

Nebot, M. and Guimerà, J.J., 2016. Structure of an inverted basin from subsurface and field data: the Late Jurassic-Early Cretaceous Maestrat Basin (Iberian Chain). *Geologica Acta*, *14*(2), 155-177.

Nenna, F. and Aydin, A., 2011. The formation and growth of pressure solution seams in clastic rocks: A field and analytical study. *Journal of Structural Geology*, *33*(4), 633-643.

Neilson, J.E., Oxtoby, N.H., Simmons, M.D., Simpson, I.R. and Fortunatova, N.K., 1998. The relationship between petroleum emplacement and carbonate reservoir quality: examples from Abu Dhabi and the Amu Darya Basin. *Marine and Petroleum Geology*, *15*(1), 57-72.

Nelson, R.A., 1981. Significance of fracture sets associated with stylolite zones: geologic notes. *AAPG Bulletin*, *65*(11), 2417-2425.

Nelson, R.A., 2001. *Geologic analysis of naturally fractured reservoirs*. Elsevier, 159.

Paganoni, M., Al Harethi, A., Morad, D., Morad, S., Ceriani, A., Mansurbeg, H., Al Suwaidi, A., Al-Aasm, I.S., Ehrenberg, S.N. and Sirat, M., 2016. Impact of stylolitization on diagenesis of a Lower Cretaceous reservoir from a giant oilfield, Abu Dhabi, United Arab Emirates. *Sedimentary Geology*, *335*, 70-92.

Railsback, L.B., 1993. Lithologic controls on morphology of pressure-dissolution surfaces (stylolites and dissolution seams) in Paleozoic carbonate rocks from the mideastern United States. *Journal of Sedimentary Research*, *63*(3), 513-522.

Rustichelli, A., Tondi, E., Agosta, F., Cilona, A. and Giorgioni, M., 2012. Development and distribution of bed-parallel compaction bands and pressure solution seams in carbonates (Bolognano Formation, Majella Mountain, Italy). *Journal of Structural Geology*, *37*, 181-199.

Rustichelli, A., Tondi, E., Korneva, I., Baud, P., Vinciguerra, S., Agosta, F., Reuschlé, T. and Janiseck, J.M., 2015. Bedding-parallel stylolites in shallow-water limestone successions of the Apulian Carbonate Platform (central-southern Italy). *Italian Journal of Geosciences*, *134*(3), 513-534.

Salas, R. and Casas, A., 1993. Mesozoic extensional tectonics, stratigraphy and crustal evolution during the Alpine cycle of the eastern Iberian basin. *Tectonophysics*, *228*(1-2), 33-55.

Salas, R. and Guimerà, J., 1996. Main structural features of the Lower Cretaceous Maestrat Basin (Eastern Iberian Range). *Geogaceta*, *20* (7), 1704-1706.

Salas, R., Guimerà, J., Mas, R., Martín-Closas, C., Meléndez, A. and Alonso, A., 2001. Evolution of the Mesozoic central Iberian Rift System and its Cainozoic inversion (Iberian chain). *Peri-Tethys Memoir*, *6*, 145-185.

Sanderson, D.J. and Nixon, C.W., 2015. The use of topology in fracture network characterization. *Journal of Structural Geology*, *72*, 55-66.

Sheppard, T.H., 2002. Stylolite development at sites of primary and diagenetic fabric contrast within the Sutton Stone (Lower Lias), Ogmore-by-Sea, Glamorgan, UK. *Proceedings of the Geologists' Association*, *113*(2), 97-109.

Tomás, S., Löser, H. and Salas, R., 2008. Low-light and nutrient-rich coral assemblages in an Upper Aptian carbonate platform of the southern Maestrat Basin (Iberian Chain, eastern Spain). *Cretaceous Research*, *29*(3), 509-534.

Toussaint, R., Aharonov, E., Koehn, D., Gratier, J.P., Ebner, M., Baud, P., Rolland, A. and Renard, F., 2018. Stylolites: A review. *Journal of Structural* Geology, 114, 163-195.

Tucker, M.E. and Wright, V.P., 2009. *Carbonate sedimentology*. John Wiley & Sons, 1-14.

Vandeginste, V. and John, C.M., 2013. Diagenetic implications of stylolitization in pelagic carbonates, Canterbury Basin, Offshore New Zealand. *Journal of Sedimentary Research*, *83*(3), 226-240.

Wanless, H.R., 1979. Limestone response to stress: pressure solution and dolomitization. *Journal of Sedimentary Research*, *49*(2).

Yao, S. (2019). *Static modelling of a shallow-marine carbonate reservoir analogue: prediction of facies distribution, sequence stratigraphy and fault-associated dolostone geometry*. Ph.D. thesis, University of Aberdeen. https://ethos.bl.uk/OrderDetails.do?uin=uk.bl.ethos.774048

Zeeb, C., Gomez-Rivas, E., Bons, P.D. and Blum, P., 2013. Evaluation of sampling methods for fracture network characterization using outcrops. *AAPG bulletin*, *97*(9), 1545-1566.